AGU PUBLICATIONS

JGR

Journal of Geophysical Research: Planets

RESEARCH ARTICLE
10.1002/2017JE005460

Special Section:
5th International Planetary Dunes Workshop Special Issue

Wind-Driven Erosion and Exposure Potential at Mars 2020 Rover Candidate-Landing Sites

Matthew Chojnacki[1], Maria Banks[2], and Anna Urso[1]

[1]Lunar and Planetary Laboratory, University of Arizona, Tucson, AZ, USA, [2]NASA Goddard Space Flight Center, Greenbelt, MD, USA

Key Points:
- Candidate-landing sites for the Mars 2020 Rover mission were assessed for potential erosion by active eolian bedforms
- Of the three downselected sites NE Syrtis then Jezero crater showed the most evidence for ongoing sand transport and erosion potential
- The Columbia Hills site lacked evidence for sand movement from local bedforms, suggesting that current abrasion rates are low

Supporting Information:
- Supporting Information S1
- Figure S1
- Figure S2
- Figure S3
- Animation S1
- Animation S2
- Animation S3
- Animation S4
- Animation S5
- Animation S6
- Animation S7
- Animation S8
- Animation S9
- Animation S10

Correspondence to:
M. Chojnacki,
chojan1@pirl.lpl.arizona.edu

Citation:
Chojnacki, M., Banks, M., & Urso, A. (2018). Wind-driven erosion and exposure potential at Mars 2020 Rover candidate-landing sites. *Journal of Geophysical Research: Planets*, *123*, 468–488. https://doi.org/10.1002/2017JE005460

Received 2 OCT 2017
Accepted 17 JAN 2018
Accepted article online 8 FEB 2018
Published online 22 FEB 2018

Abstract Aeolian processes have likely been the predominant geomorphic agent for most of Mars' history and have the potential to produce relatively young exposure ages for geologic units. Thus, identifying local evidence for aeolian erosion is highly relevant to the selection of landing sites for future missions, such as the Mars 2020 Rover mission that aims to explore astrobiologically relevant ancient environments. Here we investigate wind-driven activity at eight Mars 2020 candidate-landing sites to constrain erosion potential at these locations. To demonstrate our methods, we found that contemporary dune-derived abrasion rates were in agreement with rover-derived exhumation rates at Gale crater and could be employed elsewhere. The Holden crater candidate site was interpreted to have low contemporary erosion rates, based on the presence of a thick sand coverage of static ripples. Active ripples at the Eberswalde and southwest Melas sites may account for local erosion and the dearth of small craters. Moderate-flux regional dunes near Mawrth Vallis were deemed unrepresentative of the candidate site, which is interpreted to currently be experiencing low levels of erosion. The Nili Fossae site displayed the most unambiguous evidence for local sand transport and erosion, likely yielding relatively young exposure ages. The downselected Jezero crater and northeast Syrtis sites had high-flux neighboring dunes and exhibited substantial evidence for sediment pathways across their ellipses. Both sites had relatively high estimated abrasion rates, which would yield young exposure ages. The downselected Columbia Hills site lacked evidence for sand movement, and contemporary local erosion rates are estimated to be relatively low.

Plain Language Summary Wind-blown dune sand can wear away the Martian surface and uncover geologic units, which have not been exposed to prolonged space radiation. We studied migrating sand dunes at the eight potential Mars 2020 Rover landing sites, a mission that will explore astrobiologically relevant ancient environments. These locations may be favorable for the preservation of ancient life and organics for sampling by future Mars missions, including the Mars 2020 mission. Results indicate that candidate sites at Syrtis Major and Jezero crater showed the most evidence for ongoing sand transport and erosion potential.

1. Introduction and Motivation

The last decade of Mars exploration has revealed that the current atmosphere is capable of frequently moving surface sediment. Low-albedo aeolian sand ripples and dunes are currently migrating across the surface at many locations, while others appear static (Bourke et al., 2008; Bridges et al., 2011; Chojnacki et al., 2011; Silvestro et al., 2010; Sullivan et al., 2008). Global studies have shown geographic variations in bedform activity status (e.g., active, migrating, and no detection) based on change detection using high-resolution orbital images (Banks et al., 2015; Bridges et al., 2011). More detailed investigations have quantified volumetric sand fluxes, which are independent of dune size, for select locations on Mars (e.g., Nili Patera and Meridiani) (Bridges et al., 2012; Chojnacki et al., 2015, 2017).

Aeolian sediment flux measurements are important to our understanding of planetary surfaces as they have associated implications regarding local wind regimes, the dust cycle, and landscape evolution. Wind-driven aeolian abrasion by bedform sand also has the potential to expose geologic units for investigation by surface missions. For example, analysis by the Mars Science Laboratory (MSL) *Curiosity* rover team using in situ isotopic dating methods determined surface exposure ages of wind-eroded strata at Gale crater (Farley et al., 2014; Grotzinger et al., 2014). Sand blasting by sediment transport there has rapidly exposed potential organic-bearing sedimentary layers during scarp retreat, minimizing degradation due to cosmic rays (Farley et al., 2014). Complex organic matter on Mars would be destroyed by cosmic radiation in $<10^8$ years, unless 2–3 m of overburden were present (Farley et al., 2014; Grotzinger et al., 2014). These escarpments develop

as weaker layers are eroded and undercut by wind erosion and sand abrasion, eventually retreating downwind as part of Martian landscape evolution (Day & Kocurek, 2015; Williams & Rice, 2017). Other evidence of prolonged aeolian abrasion and deflation across Mars is evident with the common occurrence of streamlined landforms (e.g., knobs and yardangs) carved out of various terrains (Day & Kocurek, 2015; Fenton et al., 2015). Thus, assessing locales for signs of persistent surface erosion and estimating surface abrasion rates is highly relevant to future surface missions aimed at sampling materials with minimal organic degradation and possible signs of ancient life.

NASA is currently planning one such surface mission. The Mars 2020 mission has plans to launch and land a rover on the surface of Mars in that year to build on successes of prior rover missions, such as the Mars Exploration Rovers and *Curiosity* (Grotzinger et al., 2014; Squyres et al., 2003). The mission science goals outlined by the Mars 2020 Science Definition Team (Mustard et al., 2013) require a landing site that hosts a variety of characteristics for in situ investigations including anastrobiologically relevant ancient environment with biosignature preservation potential (discussed in more detail below). In this way, aeolian abrasion and erosion of the Martian surface is highly pertinent to site selection for future investigation by surface assets.

Here we investigate aeolian activity at Mars 2020 candidate-landing sites (Golombek et al., 2017) in an effort to better assess erosion and exposure potential at these locations. We begin with a summary of the 2020 landing site selection process, followed by a concise description of the approach, data, and methodology used for this investigation. We then present results related to aeolian activity at candidate-landing sites and discuss interpretations of results in the context of their relevance to Mars 2020 mission goals and other potential future landing site selections.

2. The Mars 2020 Rover Mission and Landing Site Selection

The Mars 2020 Rover mission objectives are in accordance with that of NASA's broader goal to search for signs of life in the solar system. Given this overarching strategy, the following mission objectives were defined (Mustard et al., 2013): (1) explore an astrobiologically relevant ancient environment on Mars with the assessment of past habitability, (2) search for potential biosignatures within that geological environment and preserved record, and (3) demonstrate significant technical progress toward the future return of scientifically selected samples to Earth.

To narrow down possible landing sites and maximize mission success, the NASA Mars Exploration Program held a series of landing site workshops, which included presentations and discussions from the scientific community (Golombek et al., 2017). The first landing site workshop (May 2014) identified and prioritized 27 landing sites, which were further downselected to eight and then three at the second (August 2015) and third (February 2017) workshops, respectively, largely based on community input on site science (see Golombek et al. (2017) and workshop presentations at https://marsnext.jpl.nasa.gov/index.cfm). At the time of this writing, the three remaining landing site candidates are still being assessed and more information will be presented at a forthcoming fourth workshop (anticipated for summer 2018).

For the purposes of this paper, we report on the initial eight candidate-landing sites discussed at the third workshop, as they are of great interest to the community and are potential landing sites for other future Mars missions. These sites consist of Eberswalde crater, Holden crater, Southwest Melas Chasma, Mawrth Vallis, Nili Fossae, Jezero crater, Northeast Syrtis Major, and the Columbia Hills (Gusev crater) where the last three are still under consideration (Figure 1 and Text S1 in the supporting information).

3. Aeolian Bedform Identification and Characterization for Mars 2020 Candidate-Landing Sites

3.1. Overview of Approach

In an effort to further constrain candidate-landing site geologic context and history, the work described here assessed and quantified sand movement and aeolian erosion at candidate-landing sites. For each site we utilize three approaches: (1) assess the surrounding area for regional aeolian bedform populations and determine trends in activity (section 3.2), (2) estimate regional sand fluxes (section 3.3), and (3) assess evidence for contemporary sand movement within and around candidate ellipses to determine local conditions (section 3.4). All three of these approaches largely relied on fine-scale (25–50 cm/pixel) observations from the High Resolution Imaging Science Experiment (HiRISE) (McEwen et al., 2007) on board the Mars Reconnaissance Orbiter (MRO).

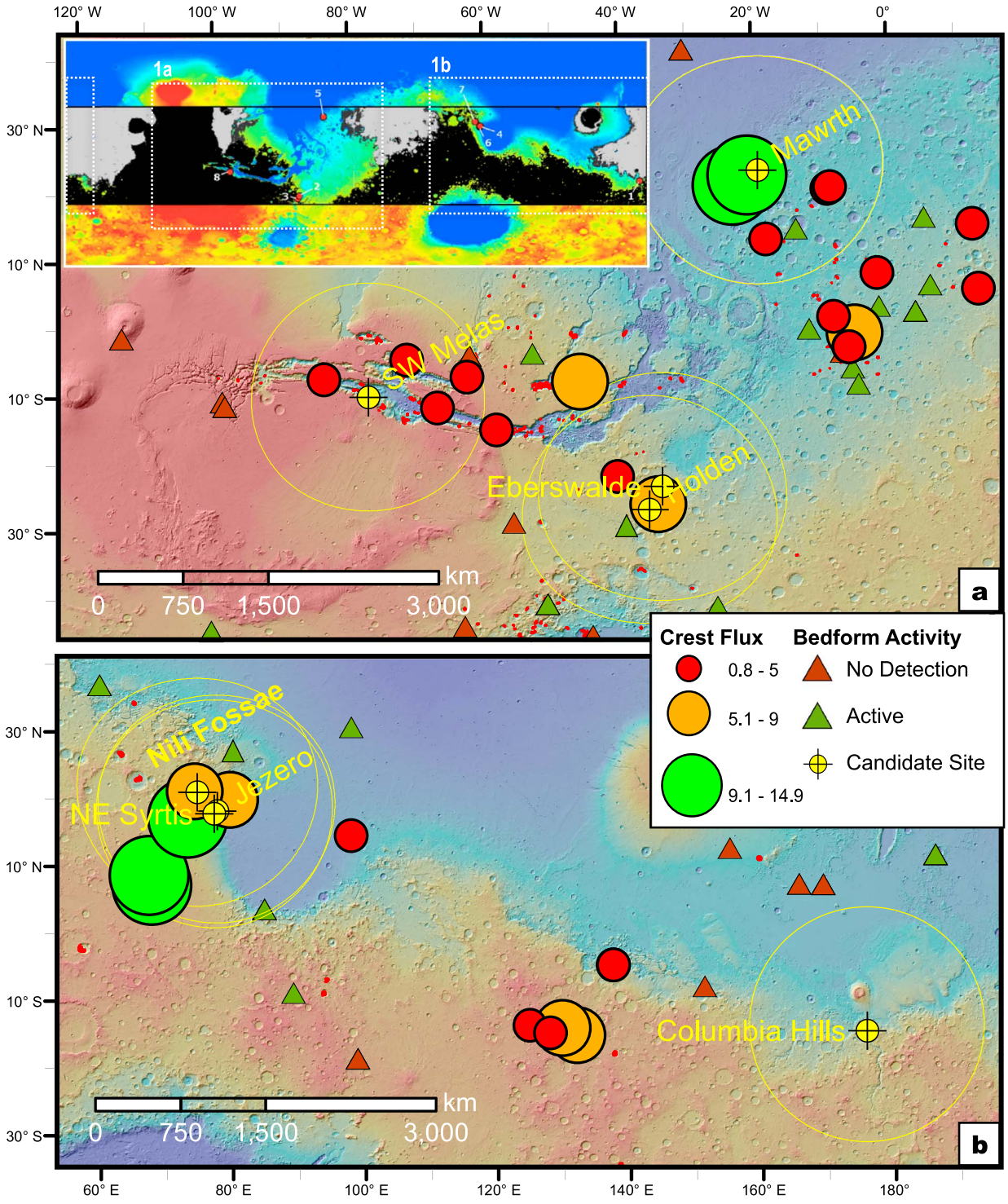

Figure 1. Subarea maps of candidate-landing sites with results from global bedform monitoring efforts and regional sand flux measurements for (a) western and (b) eastern hemispheres. Sand dune crest flux measurements (graduated circles grouped in three classes with units of $m^3\ m^{-1}\ yr^{-1}$; see Table S1). The 1,000 km radius ellipses centered on candidate sites provide scale. Base map is Mars Orbiter Laser Altimeter (MOLA) shaded relief with colorized elevation from +4 to −5 km. The distribution of dune fields (red polygons) is provided as mapped by Hayward et al. (2014) and Chojnacki et al. (2014, 2017). Figure 1a inset provides a MOLA map of Mars showing areas that meet the engineering constraints for landing the 2020 Mars rover, which are within ±30° latitude of the equator, below +0.5 km elevation, and possess surfaces with thermal inertia >100–150 $J\ m^{-2}\ K^{-1}\ s^{-1/2}$; surfaces outside of the elevation (black) and thermal inertia constraints (gray) are masked out. Areas within this latitude limit containing surfaces outside of the elevation and thermal inertia values are masked out. Locations of the candidate-landing sites (red circles) are also provided (1–8 in alphabetical order). See Golombek et al. (2017) and Figure S1 for more details. Modified from https://marsnext.jpl.nasa.gov/index.cfm.

In the first approach, we performed regional assessments of aeolian bedform populations and their mobility. This information provides context for potential mobile sediment availability and a key boundary condition for aeolian abrasion as constraints.

In the second approach, sand dune monitoring sites surrounding the candidate-landing sites were used to constrain regional sand fluxes. Prior work by Chojnacki et al. (2017) tested the hypothesis that the sand dunes in Meridiani Planum surrounding Endeavour crater, a single location previously documented to have active bedforms (Chojnacki et al., 2015), were also active and part of regional-wide sediment movement. That investigation found that all 13 Meridiani dune fields covered with repeat high-resolution data were indeed active and most were migrating broadly in the same direction with similar rates of sand flux as those in Endeavour. Thus, dune field sites established to be active from HiRISE may be a good proxy for neighboring locations (including 2020 sites) with insufficient monitoring data, potentially providing insight into local sand movement and abrasion (Chojnacki et al., 2017). As this approach relies on an assumption that regional dunes are relevant to candidate sites, which may be distant, the final approach tests that presumption and the discussion section describes further relevance.

Our third approach was to assess local conditions of candidate-landing site ellipses for contemporary aeolian bedforms. This objective was partially motivated by the fact that estimated "regional fluxes" may not be appropriate for all neighboring locations, especially when the detected migrating dunes are spatially removed from the proposed landing site. Environmental boundary conditions such as wind regime, topography, sediment supply, and sediment state can vary widely (e.g., intracrater versus plains).

3.2. Approach 1: Regional Bedform Populations and Activity

A regional assessment of the occurrences of dune fields was performed using prior results of the Mars Global Digital Dune Database (Hayward et al., 2014) and other relevant studies (Chojnacki et al., 2017; Chojnacki, Burr, & Moersch, 2014). We note that the former global database primarily identified larger, contiguous dune fields and missed smaller or more widely dispersed dunes, in part due to limited image availability. This deficiency was found mostly to impact the three sites in Syrtis Major, but all the regions surrounding the candidate sites received additional scrutiny and are discussed. Along with these populations, we utilized prior results from HiRISE monitoring efforts of aeolian bedforms (Bridges et al., 2013; Chojnacki et al., 2014, 2017, Banks et al., 2015, 2017). In the context of this report, an "active" set of bedforms showed unambiguous evidence of movement when examined with repeat observations (e.g., ripple displacement, dune lee-front advancement, and border changes). Regional bedforms may also migrate along source-to-sink sediment pathways, which are identifiable by the bedform morphology, migration direction, and other paleowind indicators (Chojnacki et al., 2014; Day & Kocurek, 2015).

It is important to recognize that there are numerous groups of aeolian bedforms on Mars, each with a very different predisposition for activity and potential for erosion. These bedforms commonly cluster into groups with characteristic length scales (e.g., wavelengths) (Lancaster, 1988). For Mars, a hierarchy of Martian aeolian bedforms is widely recognized consisting of at least three components (in order of increasing wavelengths): ripples, transverse aeolian ridges (TARs), and dunes (Bridges et al., 2011; Fenton et al., 2015). Perhaps less recognized by the broader community are the three ripple classes that are divisible by their wavelengths (tens of centimeters to tens of meters scale), particle size distributions (fine to coarse sand), and observed or inferred activities (days to thousands of years) (e.g., Bridges, Sullivan, et al., 2017; Golombek et al., 2010; Sullivan et al., 2008). The smallest class (0.05–0.20 m wavelengths) termed "impact ripples" is commonly observed at landing sites and is often observed to be mobile on the order of seasons or less (e.g., Greeley et al., 2006). Frequently associated with sand dunes, moderate-sized (2–4 m wavelengths) "dune ripples" are often observed to be active on the order of weeks to years, as observed by high-resolution orbital imaging or in situ study (Bridges, Sullivan, et al., 2017). Finally, dark "large ripples" (~5–20 m wavelengths) are often asymmetric, coarse-grained, not associated with dunes, and most are not known to be migrating today (Fenton et al., 2015; Golombek et al., 2010). TAR is a general term for larger (~20–120 m wavelengths), notably brighter Martian bedforms that typically possess a more symmetric profile and appear to be currently immobile (e.g., Chojnacki et al., 2014; Geissler & Wilgus, 2016). Low-albedo dunes, composed of sand-sized particles, are the largest bedforms (~100–600 m wavelengths), many of which are migrating today (e.g., Bridges et al., 2011). Many prior reports on the candidate-landing site regions, focusing on other aspects of the surface geology (e.g., composition and morphology) and not making these distinctions, mistakenly reported these large ripples or TARs as dunes.

3.3. Approach 2: Regional Sand Dune Fluxes

To calculate regional sand dune fluxes, we utilize two approaches based on the available image data. Where HiRISE stereo images were available, Digital Terrain Models (DTMs; 1 –m per post) were derived and used to orthorectify temporal monitoring images, determine bedform heights, and allow dune sand fluxes to be estimated (Bridges et al., 2012; Chojnacki et al., 2015, 2017). For a few locations lacking stereo data (Table S1), manual registration of subimages and a slip face length-height technique were used for bedform displacement and relief measurements, respectively, similar to prior work (Bridges et al., 2011; Chojnacki et al., 2017). Additional relevant details on both of these approaches are provided in section 1 of the supporting information.

In general, the longest-baseline image pairs were chosen for analysis, ranging up to 5 Mars years. Images in each pair were acquired at similar seasons (within ~20° of solar longitude (L_s)) and viewing geometries for optimal change detection. Image pairs that deviated from these ideal temporal settings are noted in Table S1.

To estimate migration rates, lee-front advancements were measured in orthoimages in several locations and then averaged per dune. Using the product of the migration rate (m/Earth year) and dune height (m), sediment fluxes ($m^3\ m^{-1}\ yr^{-1}$) were calculated from these two techniques (Bridges et al., 2012; Chojnacki et al., 2017). These metrics are presented as "crest fluxes" with the qualitative ranges of "Low" ($<5\ m^3\ m^{-1}\ yr^{-1}$), "Moderate," and "High" ($>9.1\ m^3\ m^{-1}\ yr^{-1}$) (also see Figure 1). Finally, all ripple fluxes were derived with estimated ripple heights of 40 cm (Bridges et al., 2012; Lapotre et al., 2016).

Crest fluxes are useful to assess landscape evolution and can be leveraged to estimate abrasion rates given certain assumptions (described in Bridges et al. (2012)). Using sediment fluxes and the abrasion susceptibility (S_a) of rocks (mass of sand needed to erode mass of rock (Greeley et al., 1982)), abrasion rates were estimated for flat to vertical target surfaces (θ = 0°–90° as vertical)). These laboratory-derived susceptibility estimates assume a basaltic composition for both the sand particles and target material (Greeley et al., 1982), but other sedimentary target materials are discussed. Abrasion rates scale with sediment fluxes and are provided in section 5.2. Additional details on crest flux to abrasion rate calculations are provided in supporting information section 2.

3.4. Approach 3: Local Assessment of Bedform Populations and Activity

In our final approach, terrains within and surrounding (~50 km) candidate-landing site ellipses were surveyed and assessed for potentially mobile surface sediment. Bedforms were mapped using the Java Mission-planning and Analysis for Remote Sensing (JMARS) (Christensen et al., 2009). Mapping was done almost exclusively using HiRISE images but was supplemented using MRO's Context Camera (CTX) data (5–6 m/pixel) (Malin et al., 2007). The candidate-landing ellipses are roughly 12 km by 10 km (Golombek et al., 2017), were provided by the USGS, and are available at JMARS.

Fortunately, due to the interest in the local geology and the process of landing site certification (Golombek et al., 2012, 2017), the candidate-landing site areas have ample HiRISE stereo and repeat coverage. Using these data, repeat image subareas were manually tied together using the nadirmost (or where available orthorectified) of the pair as the base image then "blinked" to draw out changes, similar to earlier change detection campaigns (Banks et al., 2015; Bridges et al., 2011; Chojnacki et al., 2014). Unfortunately, many repeat images were not acquired for the purposes of change detection analyses and may have offsets in seasonality of emission angles promoting parallax or shadow changes. Although we used some of these nonideal image pairs, only unambiguous changes were reported. This process allowed local surface changes to be assessed, including ripple and dune displacements, using the longest temporal baseline images available (up to 5 Mars years). In particular, analyses were focused on areas of dark ripples or sand patches, as these surfaces tend to have the highest propensity for modification due to surface winds, based on results from prior investigations (e.g., Bridges et al., 2011; Chojnacki et al., 2017). As was done with orthorectified images, change detection analysis was carried out using Exelis Visual Information (ENVI) software. Images used for the local analysis are listed in Table S2.

4. Results

In this section, we preface results with a brief description of the regional context for candidate sites followed by a description of our results for regional sediment flux and local aeolian activity. Sites are presented in their regional groups concluding with the three downselected sites from 2017.

4.1. Holden and Eberswalde Craters

Holden and Eberswalde craters are located in the ancient terrain of southern Margaritifer Terra (Figures 1 and Text S1). Many of these areas host sedimentary structures, some containing hydrated minerals, making them interesting targets for surface missions (e.g., Grant et al., 2008; Grant & Wilson, 2011; Grotzinger & Milliken, 2012; Lewis & Aharonson, 2006; Rice et al., 2011). Holden crater contains numerous alluvial fans coalescing to form bajada deposits, which were deeply eroded to display the inverted topography of distributary channel networks (Grant et al., 2008; Moore & Howard, 2005). Eberswalde also shows signs of exhumation with partially preserved putative deltaic channel deposits with distinctive lobes extending ~20 miles into the crater (e.g., Rice et al., 2013). Both of these paleolake deposits host clay-bearing minerals (Milliken & Bish, 2010) and are thought to have formed during the Hesperian period with Holden being slightly younger (Grant & Wilson, 2011).

There are 11–15 small dune fields identified in the surrounding regions of Holden and Eberswalde (Figure 2a and Table 1), typically located in craters. Two migrating dune fields, in nearby locations (<~120 km away) and with sufficient HiRISE data, have estimated crest fluxes in the low to moderate range (4–6 $m^3\ m^{-1}\ yr^{-1}$) (Figure 3, Table 1, and Text S1). Locally, Holden hosts a large dune field on the north half of the crater opposite and upwind of the landing ellipse in the southwest end of the crater (Figure 2a). Moderate-flux barchan dunes there were detected migrating to the south (6 $m^3\ m^{-1}\ yr^{-1}$) (Figure 2b and Animation S1). Other collections of barchanoid dunes and sand sheets extend west and south, with the former possessing slip faces consistent with a southward transport direction (Figure 2c). Within the Holden candidate ellipse area, no dunes or small wavelength (~5 m) rippled sand patches were identified. Dark bedforms (~10–20 m wavelengths) of large ripples, some with superposed craters, blanket much of the fan deposits within the ellipse (Figure 2d). No changes in these bedforms were observed in HiRISE temporal pairs (Figure S2, Table 2, and Text S2).

Eberswalde crater does not contain any dune fields or duneforms. Large wavelength (15–60 m), low-albedo ripples, and brighter TARs are found within the ellipse (Figure 2e), but no activity was detected in long-baseline data (e.g., 4 Mars years; Figure S2 and Table S2). Several dark-toned, wind ripple patches (3–4 m wavelengths) (Rice et al., 2013) are located several kilometers west and south of the candidate ellipse near the deltaic deposit (Figure 2f). Change detection revealed modest displacement rates of ripple crests (~0.5 m/yr) northward in a few areas (Figure S2, Table 2, Text S2, and Animation S2), indicating some propensity for sediment movement within the area.

4.2. Southwest Melas Chasma

The Valles Marineris rift system (Figures 1 and Text S1) hosts abundant sedimentary layered outcrops, hydrated minerals, and an extensive geologic record exposed in its walls making it attractive to surface missions (Golombek et al., 2012; McEwen et al., 2015; Weitz, 2003). The candidate ellipse is located in the eastern end of the well-studied enclosed basin of Southwest Melas Chasma (hereafter termed SW Melas), suggested to be a Hesperian-aged paleolake (Mangold et al., 2004; Quantin et al., 2005). The site displays distributary valley networks leading into the central basin where lower lying sets of the fan complex are interpreted to have formed in a sublacustrine environment (Mangold et al., 2004; Metz et al., 2009; Quantin et al., 2005; Williams & Weitz, 2014).

As one of the primary present-day Martian sediment sinks, the Valles Marineris region holds nearly a third of the nonpolar dune field area on Mars (Chojnacki et al., 2014). Over 80 dune fields are in the surrounding region (e.g., Ophir, Melas, and Ius), but no occurrences within SW Melas basin proper except for a few duneforms northwest of the ellipse (Figures 4a and 4c). Five regional dune fields were detected to be active, four of which were migrating with low-sediment fluxes (3–5 $m^3\ m^{-1}\ yr^{-1}$) (Figures 1a, 3, and 4b, Table 1, and Text S1). Locally, the landing ellipse and surroundings host numerous TARs (Williams & Weitz, 2014), but none were detected to be active. Smaller dark-toned, sand ripple (~4 m wavelengths) are often lining topographic lows and often mobile (Figures 4d and S2, Tables 2 and S2, and Animation S3), similar to ripples in nearby Ius Chasma (Chojnacki et al., 2014).

4.3. Mawrth Vallis

The Mawrth Vallis (Figure 1 and Text S1) is a large outflow channel, which exits into the northern lowlands and bisects light-toned, stratified bedrock dated to be Early to Middle Noachian in age (Bibring et al., 2005;

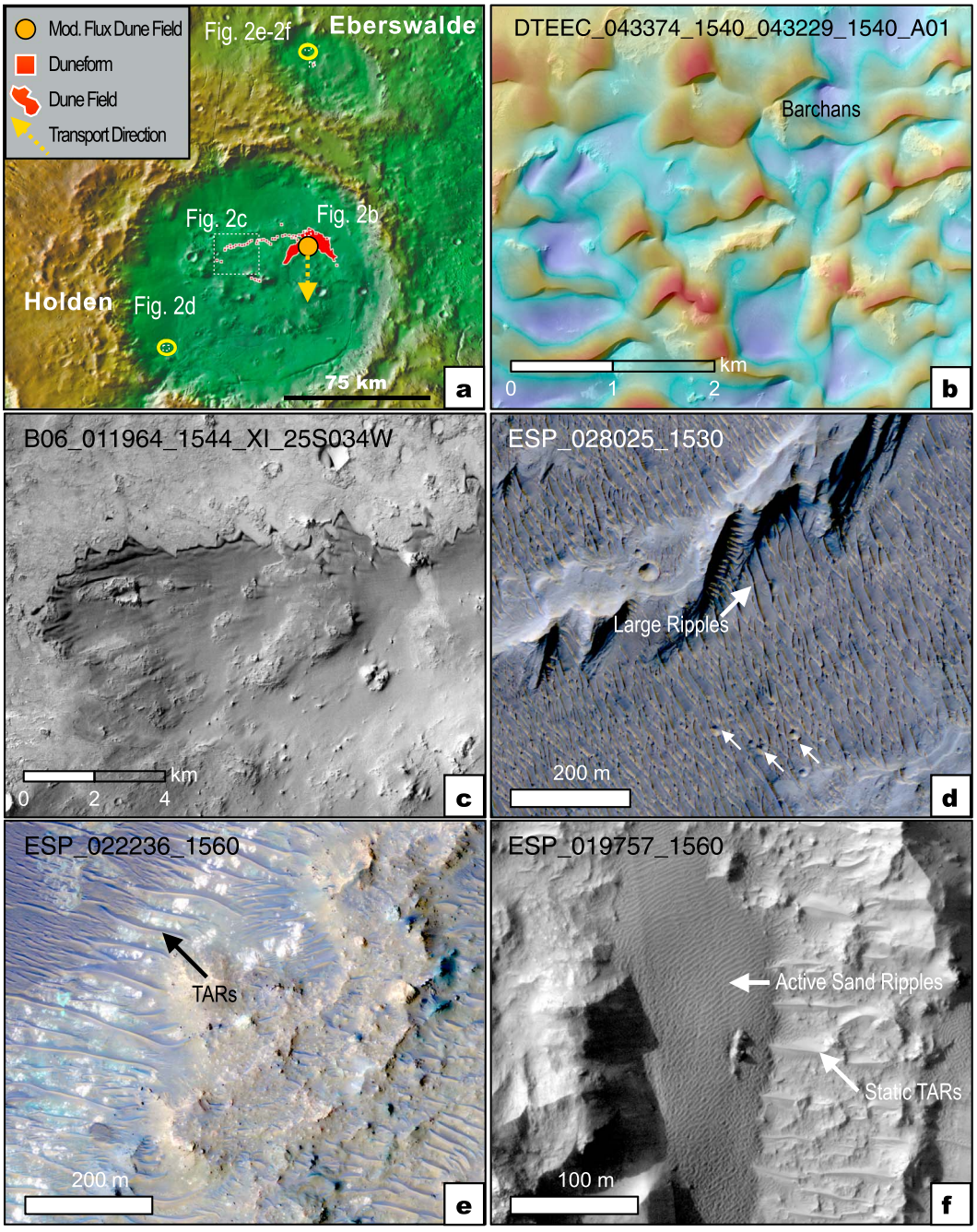

Figure 2. Candidate-landing sites at Eberswalde and Holden craters. (a) Regional context showing locations of landing ellipses (yellow) and Figures 2b–2f. Contiguous dune fields (red polygons) and more diffuse individual dunes (red squares) are shown. THEMIS Day-IR colorized with MOLA elevation from +4 to −5 km. Panels in Figures 4–9 have similar symbology and subfigures are all oriented with north up unless noted. (b) Holden barchanoid dunes detected migrating south and toward the landing ellipse. HiRISE orthoimage ESP_043374_1540 colorized with elevation from the host DTM (also see Animation S1). (c) Central Holden dunes distributed broadly upwind of the landing ellipse (CTX). (d) Inverted channels within the Holden landing ellipse with superposed (inactive) megaripples, cratered in places (white arrows; (HiRISE IRB color). (e) Eberswalde landing ellipse area with numerous static TARs found to be inactive (HiRISE IRB color). (f) Small, isolated bedform units of mobile wind ripples found south of the ellipse (HiRISE RED; also see Animation S2).

Bishop et al., 2008; Loizeau et al., 2007; Michalski & Noe Dobrea, 2007; Poulet et al., 2005; Wray et al., 2008). The Mawrth candidate ellipse is located on the plateau to the west where widespread Al-phyllosilicates and hydrated-silica materials are overlaid by a resistant, low-albedo capping unit, all of which possess a

Table 1
Summary of Mars 2020 Candidate-Landing Site Regional Results

	Regional dune fields[a,b]		Bedform monitoring sites[c]		Sediment flux		Regional summary[d]
Candidate site	Num.	Ave. area (km^2)	Active	Migrating	Num./min. distance (km)	Flux ave. ($m^3\ m^{-1}\ yr^{-1}$)	
Holden	11	32.0	3	2	2/87.5	5.3	Moderate
Eberswalde	15	122.1	2	2	2/163.9	5.3	Moderate
SW Melas	82	354.5	5	4	4/420.6	4.0	Low
Mawrth	11	112.4	7	7	5/101.8	5.6	Moderate
Nili Fossae	11	425.2	7	5	5/18.7	11.6	High
Jezero	11	483.2	8	5	5/144.8	11.6	High
NE Syrtis	11	483.2	8	5	5/183.9	11.6	High
Columbia Hills	0	0	0	0	0/–	-	-

[a]Statistics collected within the 1,000 km ellipses and centered on candidate sites. [b]Data collected from the Mars Global Digital Dune Database polygons available from the USGS (Hayward et al., 2014) and earlier mapping by Chojnacki et al. (2014, 2017). [c]Dune mapping results from Banks et al. (2017) and herein. [d]Qualitative sediment fluxes are defined as the following: "low" (<5 $m^3\ m^{-1}\ yr^{-1}$), "moderate," and "high" (>9.1 $m^3\ m^{-1}\ yr^{-1}$).

debated origin (e.g., fluvial, lacustrine, altered volcanic ash, aeolian, and impact deposits) (Grotzinger & Milliken, 2012; Michalski & Noe Dobrea, 2007). Mawrth was one of the final four downselected landing sites for MSL, along with Eberswalde, Holden and Gale crater (Golombek et al., 2012), and a candidate 2020 ExoMars Rover landing site (Bridges, Loizeau, et al., 2017), attesting to its intriguing geology.

Eleven regional dune fields primarily occur to the southeast of the Mawrth site (Meridiani and Arabia Terra), but in nearby Oyama and McLaughlin craters to the southwest (Figures 1a and 5a, Table 1, and Text S1). These dune fields, along with five others, have migrating dunes with low- to high-sediment fluxes (1–12 $m^3\ m^{-1}\ yr^{-1}$) (Figures 3 and 5b and Animation S4). All of these dune fields are found in intracrater environments rather than the higher plateau regions (Figure 5a). These plateau areas and the landing ellipse have bedforms covering an estimated ~20% of the surface (Bridges, Loizeau, et al., 2017). However, all of these local bedforms are large wavelength (~20–30 m), bright TARs (typically clustered in craters) and large (~8–20 m), dark-toned ripples (Figures 5c and 5d). In both cases, no displacements of bedform crests were detected within and adjacent to the landing ellipse in long-baseline HiRISE pairs (4–5 Mars years; Figure S2, Table 2, Text S2, and Animation S5).

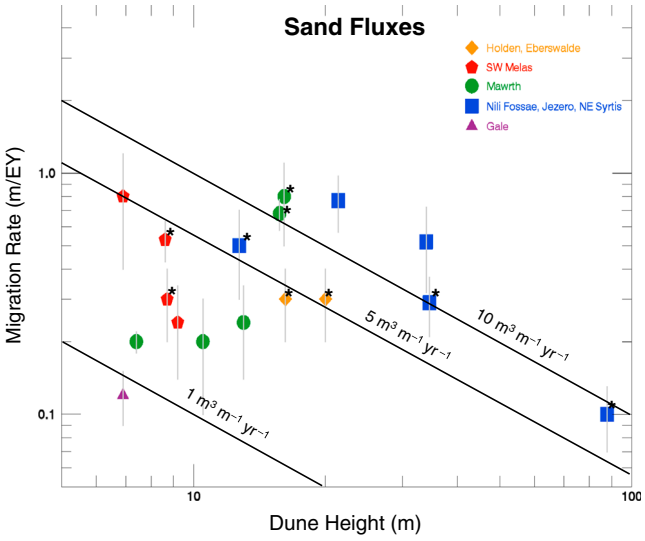

Figure 3. Comparison of dune migration rates versus heights for Mars 2020 candidate site regional sand dunes. Plot is in log-log space, and diagonal lines are isopleths of sand flux. Migration rates for dunes in the study areas are averages using the longest baseline images available. Monitoring sites within 500 km of a given candidate-landing site are indicated with a "*" and the standard deviations of crest fluxes for a given group of dunes are indicated by vertical error bars (typically ±0.1–0.3 m/yr). Additional data plotted are dunes at Gale crater from Chojnacki et al. (2017). See Table S1 for image and site information.

4.4. Nili Fossae

The Nili Fossae consists of a group of large, broadly concentric grabens, located in the Syrtis Major region and adjacent to the~4 Ga Isidis impact basin in the east (Figure 1 and Text S1) (Mustard et al., 2007). The region has been noted of interest as the fossae bisects and exposes several hundreds of meters of phyllosilicate- and ultramafic-bearing Noachian crust (e.g., Bibring et al., 2005; Poulet et al., 2005). This crust is also superposed by extensive Syrtis Major lava units that preserve geologic elements of the Hesperian-Noachian boundary (Ehlmann et al., 2009; Grotzinger & Milliken, 2012; Hoefen et al., 2003; Mustard et al., 2007). Additional trough fill material includes Hargraves crater and Isidis impact ejecta, reworked crustal clay and carbonate materials, and substantial unconsolidated basaltic sand (Grotzinger & Milliken, 2012).

Global mapping efforts identified 11 dune fields distributed across the broader Nili Fossae/Syrtis Major region, often within nearby craters and patera (e.g., Nili Patera; Table 1) (Hayward et al., 2014). At least seven of these occurrences were detected to be active, with five migrating with moderate to high average sediment fluxes (7–17 $m^3\ m^{-1}\ yr^{-1}$) (Figures 1b, 3, and 6b and Table S1). Additional dune fields not captured in prior mapping efforts are located both

Table 2
Summary of Mars 2020 Candidate-Landing Site Local Results[a]

Location	Local bedform change[b]?	Notes[c]	Qualitative assessment[d]
Holden	No	Large moderate-flux (4–6 $m^3\ m^{-1}\ yr^{-1}$) dune field in Holden to north (upwind). other dunes in central crater that appear to be active from the same northerly wind regime. Megaripples dominate the ellipse area (some with craters) and are interpreted to be inactive and coarse grained. No evidence of contemporary sand movement in ellipse area.	Low
Eberswalde	Yes	Clear movement of several small ripple patches on west and south edge of ellipse (~0.5 m/yr; 0.1 $m^3\ m^{-1}\ yr^{-1}$). No evidence of contemporary sand movement in ellipse from megaripples or TARs, nor are any dunes present in the basin.	Moderate
SW Melas	Yes	Minor (active) sand patches within and adjacent to the ellipse (~0.5 m/yr; 0.1 $m^3\ m^{-1}\ yr^{-1}$). Numerous regional (active) dune fields, but none local. Only minor duneforms in SW Melas basin proper (to the west).	Moderate
Mawrth	No	High flux dune fields located in craters to the west. Only TARs and megaripples are present on the plateau and ellipse areas. No evidence for bedform changes.	Low
Nili Fossae	Yes	Numerous dune fields to SW-NW and generally downwind of ellipse are active. Scattered dunes on plateau to east (upwind) and Hargraves crater dune field. Good evidence for sediment pathways of moderate flux dunes (~7 $m^3\ m^{-1}\ yr^{-1}$) across the proposed ellipse.	High
Jezero	Yes	Numerous dunes on the plateau to north, west, and east (upwind), some of which are active. Large high-flux dune fields in crater to the NE and low flux dunes in Jezero inlet channel. Minor (active) sand ripples adjacent to fan (~0.2 m/yr; 0.04 $m^3\ m^{-1}\ yr^{-1}$).	High
NE Syrtis	Yes	Numerous dunes on the plains to north, west, and east (upwind), some of which are active (1.8 $m^3\ m^{-1}\ yr^{-1}$). Good evidence for sediment pathways across the proposed ellipse.	High
Columbia Hills	No	Numerous patches of sand ripples, mostly within small craters, including within the ellipse. No detections of bedform change other than small impact ripplesobserved by Spirit.	Low

[a]Also see Table S1 and Figure S1. [b]Detected bedform changes in or within 10 km of candidate ellipse. [c]All sites have aeolian bedforms (transverse aeolian ridges (TARs) and small/megaripples) within the proposed landing ellipse. [d]"Low" indicates that no local changes were detected. "Moderate" indicates that at least small ripples were detected migrating. "High" indicates sites with migrating dunes adjacent to the ellipse and some evidence for sediment paths across the ellipse.

locally within the trough and the adjacent plateau areas (Figures 6 and 7a). These occurrences include a large moderate-flux dune population a few kilometers to the northwest and downwind of the ellipse (Figure 6d, Table S1, and Animation S6). Similarly, dark dunes to the southeast of the ellipse and aligned against the western border of the main fossa are also migrating via the same southeasterly wind regime (Figure 6c, Text S2, and Table S2). While the candidate ellipse exhibits less sandy sediment than the western edge of the trough, it does contain some dark rippled patches that also showed changes (Figure S2 and Table S2).

4.5. Jezero Crater and Northeast Syrtis Major

The Syrtis Major area wedged between Isidis to the east and fossae to the west contains shallow grabens and craters that expose the heavily altered crust and has become of great interest to the Mars community (e.g., Bramble et al., 2017; Ehlmann et al., 2009; Grotzinger & Milliken, 2012; Mustard et al., 2007). It also hosts two of the final three downselected candidate 2020 landing sites—namely, Jezero crater and Northeast Syrtis Major (hereafter termed NE Syrtis) (Figure 7a). Jezero includes a well-preserved (putative) delta complex with carbonate and phyllosilicate signatures and the potential for a deep lacustrine environment thought to postdate the late Noachian Isidis impact event (e.g., Ehlmann et al., 2008; Fassett & Head, 2005; Goudge et al., 2012). The NE Syrtis site is just as ancient and spectrally diverse (e.g., carbonates, sulfates, phyllosilicates, and igneous minerals) but includes well-exposed megabreccia blocks and geologic terrain, which have been hypothesized to represent an ancient, subsurface-aquifer and serpentinizing system (Baratoux et al., 2007; Bramble et al., 2017; Edwards & Ehlmann, 2015; Ehlmann et al., 2009).

The Jezero and NE Syrtis candidate-landing sites are both surrounded by many aeolian landforms (Figures 1b, 7, and 8, Tables 1 and 2, and Text S1). For example, the large crater, a few hundred kilometers to the northeast of Jezero, has a field of particularly large (~80–120 m tall) moderate-flux dunes (8 $m^3\ m^{-1}\ yr^{-1}$) (Figures 3 and 7b and Table S1). However, unlike the majority of nonpolar dunes on Mars, most regional sand dunes are distributed across the Syrtis plateau rather than contained in craters or depressions (Figure 7a and 8a). These discrete collections of sand dunes commonly form "barchan trains" broadly aligned westward (Figures 7a and 8a). Similar to many of the shallow valleys crossing the Syrtis plains, the inlet and outlet channels of Jezero have small barchans (Bramble et al., 2017)—those in the northern inlet valley were detected

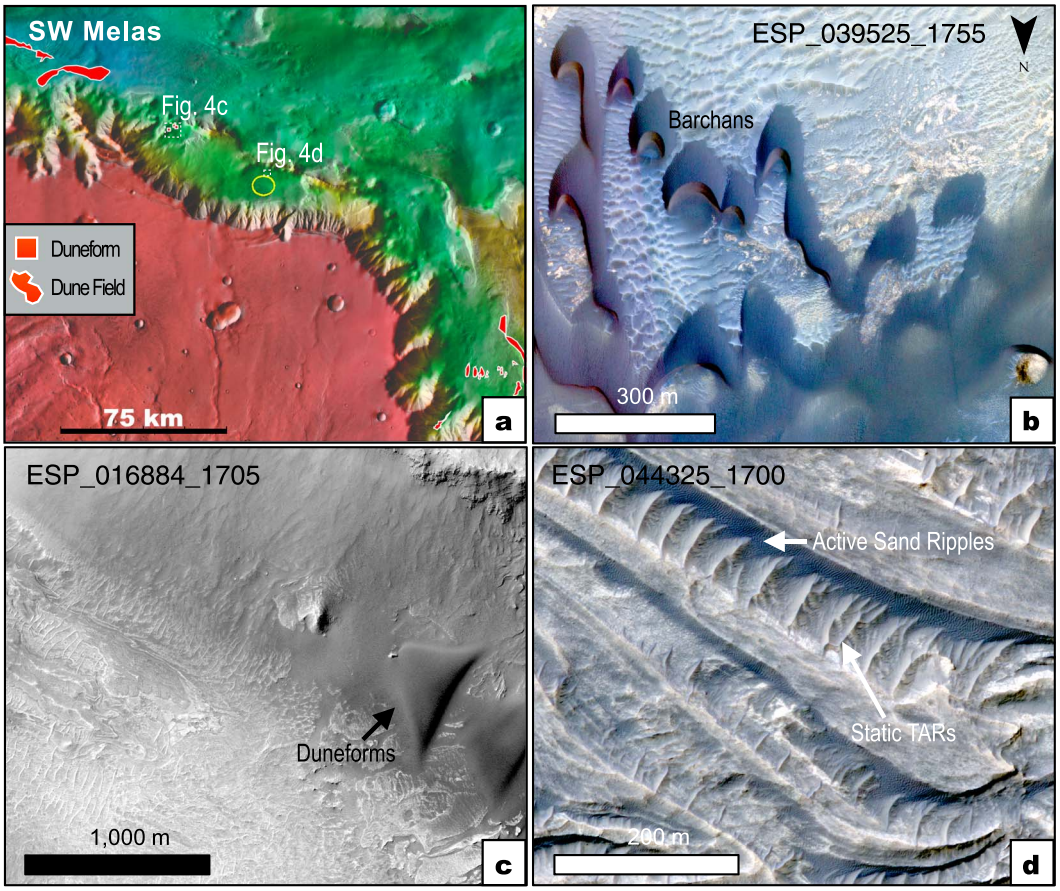

Figure 4. Candidate-landing site at SW Melas Chasma. (a) Similar to Figure 2a. (b) Ophir Chasma barchan and barchanoid dunes detected to be migrating north (HiRISE IRB color). (c) Several small dunes within the Melas basin, west and broadly upwind of the landing ellipse (HiRISE RED). (d) Light-toned layered units adjacent to the ellipse, where static TARs are superposed by active ripple beds (HiRISE IRB color; also see Animation S3).

migrating west with low fluxes (1.8 m^3 m^{-1} yr^{-1}), atop static TARs (Figures 7c and S2, Tables 2 and S2, and Animation S7). This primary easterly wind regime appears to be responsible for driving most of the aeolian regional indicators, including the dark and light streaks upwind of the Jezero and NE Syrtis sites (Figure 8c). Jezero crater does not contain any veritable sand dunes, but there are numerous large ripples and TARs within the ellipse and basin—those showed no movement. Smaller wind rippled patches (3–4 m wavelengths) located in the landing ellipse and at the delta toe were detected to be mobile with rates of ~0.2 m/yr (Figures 7d and S2, Tables 2 and S2, and Animation S8).

As mentioned above, the plateau surrounding the NE Syrtis landing zone also exhibits numerous sand dunes and wind streaks. The vast majority of these features appears to be formed by the same easterly wind regime, including migrating dunes to the southeast (Figure 8 and Animation S9). Within the NE Syrtis ellipse no dunes occur, but ample dark, potentially mobile sediment is present (Figure S2, Table 2, and Text S2).

4.6. Columbia Hills

Gusev crater contains a hypothesized paleolake formed when the Ma'adim Vallis channel system fed water from the southern highlands and breached the southern rim (Figures 1 S1, and S3) during the Early to Middle Noachian period (Arvidson et al., 2006; Crumpler et al., 2011). The crater interior was visited by the MER-*Spirit* and revealed a protracted history in which basaltic volcanic resurfacing of the Gusev plains was followed by impact and, to a lesser extent, aeolian processes (Arvidson et al., 2006; Greeley et al., 2006). The geology became more complex when *Spirit* traversed into the older Columbia Hills and encountered compositional heterogeneity with opaline silica, phyllosilicates, and carbonate exposures associated with possible pyroclastics, lacustrine, and hydrothermal deposits (Crumpler et al., 2011; Morris et al., 2010; Ruff

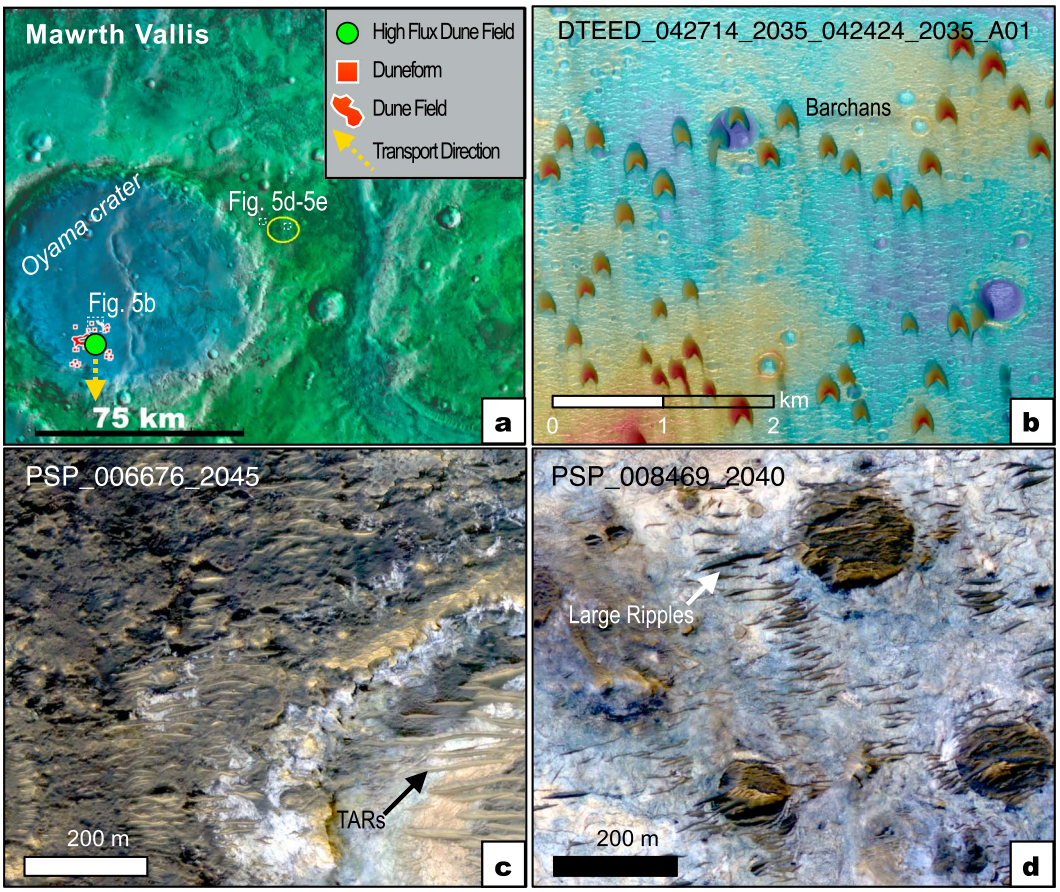

Figure 5. Candidate-landing site at Mawrth Vallis. (a) Similar to Figure 2a. (b) High sand flux sand dunes adjacent to the landing ellipse in Oyama crater (also see Animation S4). HiRISE orthoimage ESP_042714_2035 colorized with elevation from HiRISE DTM. (c) Area of the Mawrth plateau west of the landing ellipses displaying the mafic capping unit that intersects a crater with bright, static TARs (located along HiRISE IRB color). (d) Clay-bearing light-toned area within the ellipse superposed with dark, smaller wavelength ripples or TARs, which did not show evidence for migration (HiRISE IRB color; also see Animation S5).

et al., 2011). Following the Spirit mission conclusion in 2010, new data analysis and terrestrial field work revealed Columbia Hill's geological and astrobiological importance, ultimately elevating it to being a Mars 2020 candidate-landing site (Ruff et al., 2017; Ruff & Farmer, 2016).

No dune fields were mapped in the broader region out to ~1,500 km (Hayward et al., 2014), nor were any identified herein (Figures 1b and S and Table 1). The highland regions to the south (e.g., Terra Cimmeria) do have dune fields, but not at this longitude, whereas the northern lowlands (e.g., Lucas Planum) only have isolated dunes in large, distant (>1,600 km) craters (e.g., Petit crater) (Figure S3). Prior global bedform monitoring efforts only identified locations with static TARs (Banks et al., 2015; Bridges et al., 2011). Our regional survey did locate numerous dark streaks and dust devil tracks, which have been previously documented to form and fade in Gusev, indicating some sediment transport (Arvidson et al., 2006; Greeley et al., 2006). More locally, dark sand ripple patches with wavelengths 2–5 m in length were identified. These occur within or adjacent to shallow craters along the plains or on the southern sides of Columbia Hill's terrain (Figures 9a and 9b and S2). One of these latter occurrences was visited and investigated by the *Spirit* rover. The "El Dorado" campaign documented small (~3 m wavelengths, ~30 cm tall) dark bedforms that were identified to be coarse-grained, static-ripples based on the grain size distribution and lack of sediment mobility, except for dust removal (Sullivan et al., 2008). HiRISE-based analysis of El Dorado and neighboring ripple fields (Figure 9c) using long-baseline images (i.e., 4–5 Mars years) did not identify crest displacements (Tables 2 and S2 and Animation S10). Several other ripple fields along the plains and candidate ellipse did not show changes except for subtle variations in tone and dust

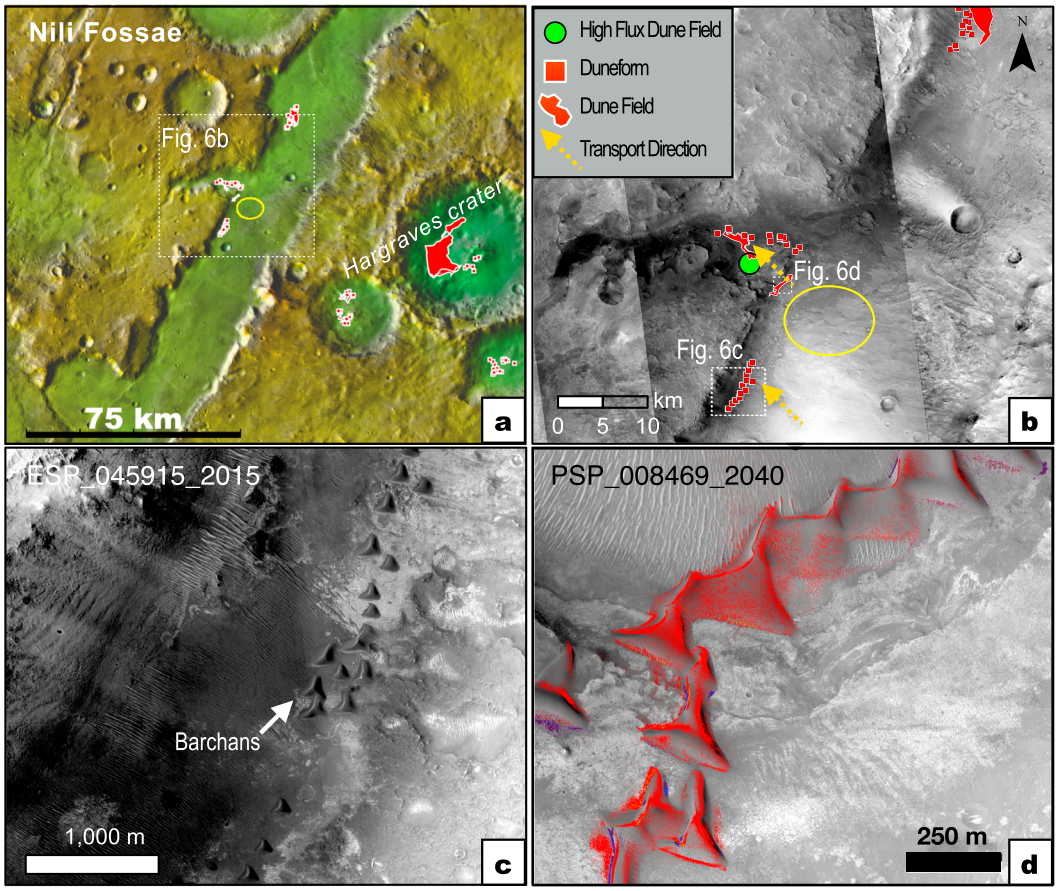

Figure 6. Candidate-landing site at Nili Fossae. (a) Similar to Figure 2a. (b) A closer view of the immediate area surrounding the ellipse where dunes line the west portions of the trough. Locations of other figures are noted. CTX mosaic. (c) Areas southwest of the ellipse where numerous migrating sand dunes and ripples occur (HiRISE RED). (d) Displacement map of rapidly advancing barchans (~1 m/yr) on the northeast edge of the landing ellipse. Red-yellow areas indicate darkening (lee-front advancement), while purple-green show lightening (stoss side advancement) over ~4 Mars years (also see Animation S6).

devil tracks (Figures 9d and S2 and Table S2), consistent with prior surface observations (Sullivan et al., 2008). However, *Spirit* did detect migrating impact ripples (wavelengths of 10 cm and unresolvable by HiRISE) during the 2007 global dust storm (Sullivan et al., 2008).

5. Discussion: Synthesis of Results and Implications

5.1. Assessment of Aeolian Activity at Candidate Mars 2020 Landing Sites

Here we evaluate and interpret results to better assess the dearth or prevalence of aeolian activity for Mars 2020 candidate-landing sites. Ultimately, we intend to address the questions: Are the regions surrounding candidate-landing site areas known to have active bedforms and how relevant are those locations to the site? Do the candidate ellipses show evidence for local aeolian transport?

5.1.1. Holden and Eberswalde

Moderate regional sediment fluxes were found for the Holden and Eberswalde sites, including several fields north and upwind of the Holden ellipse (Figures 1a, 2, and 3). No evidence of local sand movement was found in or around the Holden ellipse. Large (static) ripples blanket much of the ellipse protecting it from sand erosion (Figure 2d)—based on the similarities to Meridiani immobile bedforms studied by the MER-*Opportunity* rover (e.g., wavelength and superposed craters), these are interpreted to be coarse-grained ripples (Golombek et al., 2010). The inverted channels exposed on the Holden fan complex indicate that large-scale erosion has occurred.

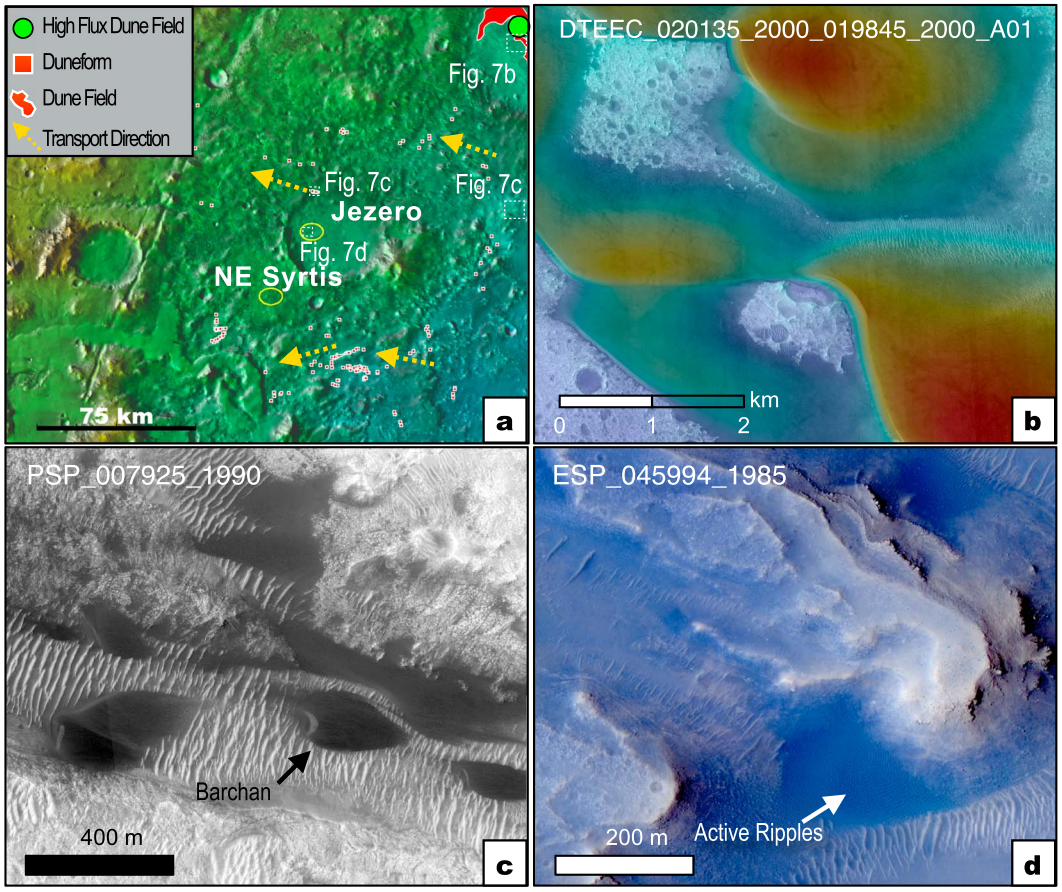

Figure 7. Candidate-landing sites at Jezero and NE Syrtis. (a) Similar to Figure 2a. (b) High sand flux sand dunes a few hundred kilometers to the northeast of the Jezero landing ellipse. Note the scale of the large 80–120 m tall dunes as compared with smaller, faster dunes shown at the roughly the same scale as Figures 2b and 4b. HiRISE orthoimage ESP_020135_2000 colorized with elevation from its parent HiRISE DTM. (c) A dry river inlet channel entering the north rim of Jezero with active dunes migrating west. Underlying TARs are static (HiRISE RED; also see Animation S7). (d) Small patches of wind ripples located along the delta toe and within the Jezero ellipse. The darker ripples are active, while the brighter underlying bedforms are not (HiRISE IRB color; also see Animation S8).

Eberswalde crater does not contain any sand dunes but does include TARs and large ripples that appear inactive. Several patches of sand ripples were identified to be migrating on the edge of ellipse (Figure 2f and Table S2). Although spatially limited in their extent (Rice et al., 2013), these ripples indicate that some mobile sediment is available and may be contributing to local erosion. These mobile ripples are frequently associated with delta-deposit scarps where evidence of boulder calving and scarp erosion has been found (Williams & Rice, 2017). Other escarpment patterns were identified in the area and may be indicative of geologically recent scarp retreat, similar to Gale (Williams & Rice, 2017).

5.1.2. SW Melas

Valles Marineris has numerous migrating dune fields, primarily with low fluxes, but none occur in SW Melas (Figures 1a, 3, and 4). Static TARs and candidate paleomegaripples (Williams & Weitz, 2014) are most common within the basin interior. However, numerous smaller mobile ripples were also identified, including within the ellipse (Figure 4d and Table S2). The local terrain is otherwise relatively flat with occasional knobs and would allow interbasin aeolian sediment transport.

5.1.3. Mawrth

The Mawrth Vallis region possesses many low- to high-flux dune fields, some of which are adjacent to the candidate site (Figures 1a, 3, and 5). However, none of these dunes occur on the Mawrth plateau region that hosts the candidate-landing zone and thus these dunes are not good indicators of the local environment. Extracrater dunes do occur on Mars, but less frequently, and are particularly rare in Arabia Terra

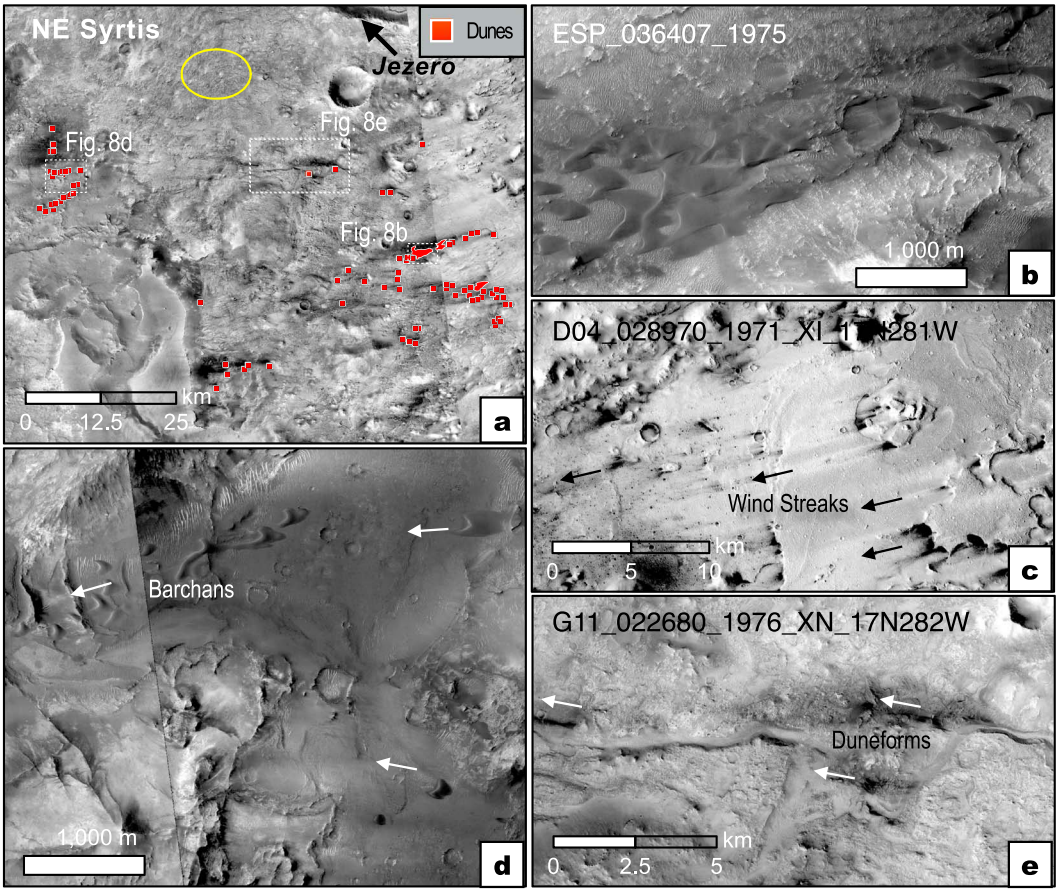

Figure 8. Candidate-landing site at NE Syrtis. (a) Regional context showing locations of landing ellipse (yellow) and other figures. CTX mosaic. (b) Typical regional barchan and barchanoid dunes found southeast of the ellipse arranged with slip faces facing east. Based on the crisp dune crests and propensity of other local dunes, these are likely active (HiRISE RED). (c) Bright and dark wind streaks directly east of Jezero and formed by the same easterly wind regime. See Figure 7a for location. CTX image. (d) Regional dunes to the southwest of the ellipse with slip faces facing to the west and east (arrows), suggesting shifting or seasonal wind regimes (also see Animation S9). HiRISE ESP_038029_1980(west), ESP_026280_1975 (east) RED images. (e) Barchan dunes and dark sand streaks in near a small channel east and upwind of the NE Syrtis ellipse (HiRISE RED).

(Chojnacki et al., 2017; Hayward et al., 2014). The ellipse area does contain many TARs and (likely coarse-grained) megaripples (Figures 5c and 5d), but these were not detected to be active, consistent with the notion that these features are not contemporary (Chojnacki et al., 2014; Fenton et al., 2015; Geissler & Wilgus, 2016; Golombek et al., 2010). Consequently, the site yielded very little compelling evidence for ongoing bedform migration and associated erosion.

5.1.4. Nili Fossae

Nili Fosse contains prominent moderate-flux dunes, including those adjacent and downwind of the candidate ellipse (Figures 1b, 3, and 6). These dunes would have migrated across and eroded the ellipse terrain if regional winds were consistent over the recent past (e.g., thousands of years). The landing ellipse environment was also found to show evidence for sand transport and long-termed erosion. These migrating bedforms were deemed responsible for removing dust that would otherwise mask the prominent spectral detections of mafic and clay materials associated with bedrock surfaces in Figure 6b (Mustard et al., 2008).

5.1.5. Jezero and NE Syrtis

The plateau surrounding the Jezero and NE Syrtis sites contains strong evidence of contemporary wind indicators with dark streaks, ripples, and high-flux regional dunes (Figures 1b, 3, 7, and 8). Although Jezero does not contain dunes, there are some within inlet and outlet valleys that may form a sediment pathway through

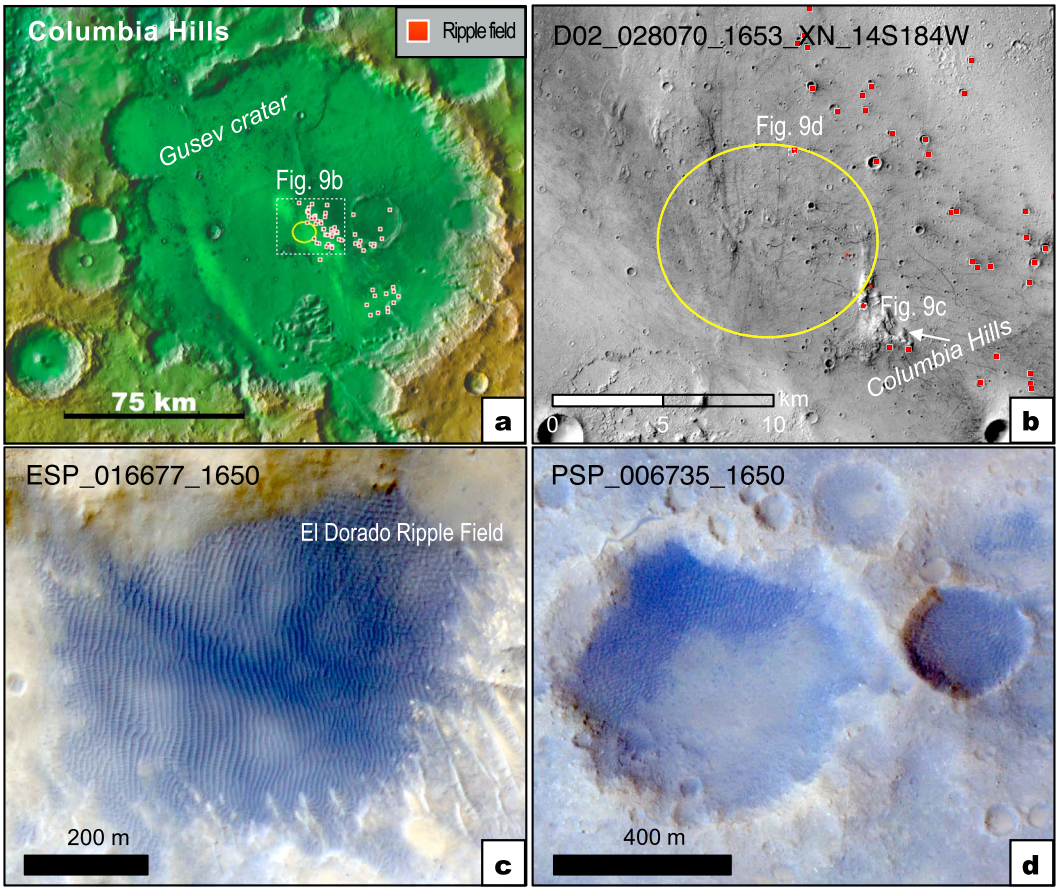

Figure 9. Candidate-landing site at the Columbia Hills, Gusev crater. See Figure S2 for wider regional context. (a) Similar to Figure 2a. (b) A closer view of the immediate area surrounding the ellipse where ripple fields can be found (red squares). CTX mosaic. (c) The El Dorado coarse-grained ripple field previously visited by the Spirit rover in 2007. Ripples were not detected to be active here and elsewhere in the region (also see Animation S10). (d) Ripples found within craters and occasionally on the adjacent plains (upper rights).

the crater. Ripples within the Jezero ellipse, detected to be migrating via the same easterly regional wind regime as those on the plateau, support this notion (Animation S7).

The NE Syrtis site likewise appears to possess broad westward sediment pathways adjacent to and across the landing area as evident by the presence of active sand streaks, ripples, and dunes. Although small craters and troughs populate much of the plateau, these do not appear prohibitive to sand transport. This region also bears some of the most prominent spectral signatures and color diversity across the planet, often adjacent to aeolian bedforms (Bramble et al., 2017; Ehlmann et al., 2009).

5.1.6. Columbia Hills

The vast areas surrounding Gusev crater do not contain dune fields (Figure S3), indicating that boundary conditions are not conducive for large-scale aeolian sediment pathways in the region. While episodic dark streaks do occur within Gusev, their changes are primarily attributed to dust devil sediment redistribution rather than horizontal wind sheer and sand saltation (Arvidson et al., 2006; Greeley et al., 2006). The numerous, but spatially limited, dark ripple beds and TARs within the ellipse and in the Columbia Hills are not mobile based on a decade of observations from orbit and from the surface (Sullivan et al., 2008) (Figure 9, Table S2, and Animation S10). *Spirit* observations of the Gusev plains (e.g., equally spaced clasts and dominant coarse-sand population) were interpreted to indicate limited sand transport and erosion (Arvidson et al., 2006). In contrast, numerous geologic units within the Columbia Hills yielded evidence for protracted aeolian and mass-wasting erosion, along with the area having a lower crater density and generally weaker rock strengths relative to the plains (Crumpler et al., 2011; Thomson et al., 2013).

5.2. Potential Surface Aeolian Erosion at Mars 2020 Candidate Sites and Examples From Gale Crater

Direct knowledge of the presence, activity, and amount of sand movement obtained from HiRISE data can elucidate the relative magnitude of sand erosion in those areas. However, it would be useful to compare our methodology to other independent techniques of inferred rock exhumation rates. As a case study we can briefly look at Gale crater, which does have active dunes near where contemporary scarp retreat and erosion rates have been documented (Grotzinger et al., 2014; Silvestro et al., 2013). Cosmogenic dating of samples at Yellowknife Bay showed that local sedimentary scarps are retreating at an average rate of ~0.75 μm/yr (Farley et al., 2014). Migrating Gale sand dunes are modest in scale and celerity, yielding low-fluxes (~1 m^3 m^{-1} yr^{-1}) (Chojnacki et al., 2017). Extrapolating these fluxes to interdune field abrasion rates of local basaltic bedrock (supporting information section 2) would equate to 0.1–1.3 μm/yr for flat ground and 1.3–6.6 μm/yr for a vertical rock face (note that m/Myr is equivalent to μm/yr). These estimates bracket the one for Yellowknife Bay and are comparable to earlier assessments of surface erosion on Mars (e.g., Golombek et al., 2006; Kite & Mayer, 2017). Dune sand is not currently abrading Yellowknife units and has (presumably) passed downrange, so that might account for the larger estimated abrasion values (i.e., >0.75 m/Myr). Other Gale deposits have been mapped from the surface and orbit and indicate that scarp retreat has occurred in a similar direction as was the case at Yellowknife Bay (Williams & Rice, 2017). These findings indicate that locations with modern bedforms, even with low-sediment fluxes, can show substantial evidence for contemporary aeolian abrasion and provide insight into long-term landscape exhumation.

Here we discuss how this approach might be applicable to Mars 2020 candidate-landing sites to determine if abrasion rates will yield potentially low exposure ages for sampling. All four of the fluvial-sedimentary sites (e.g., Holden, Eberswalde, Melas, and Jezero) show erosional remnants of their deposits that are commonly attributed to aeolian deflation (Grotzinger & Milliken, 2012), but are contemporary observations at all consistent with present-day aeolian erosion? If the sand supply and northerly wind regime in Holden were consistent in the past, we can expect sand movement toward and across the ellipse. Assuming contemporary conditions of the upwind dunes (e.g., Figures 2b and 3), slightly higher abrasion rates than at Gale would have operated there in the past. That scenario would help explain the necessary erosion required for the removal of the tens to hundreds of meters of terrain and inverted topography present on the fan today (Figure 2d) (Grant et al., 2008). Currently though, ~60% of the Holden ellipse is mantled by considerable sand coverage with static ripples with superposed craters. This sediment may shelter much of the deposit from erosional processes resulting in long exposure ages. However, interripple areas may be experiencing some limited aeolian erosion from mobile fine sediment despite larger bedforms appearing static, similar to the localized exhumation of the Burns Formation at Meridiani (Golombek et al., 2014).

Eberswalde ripples (Figure 2f) with estimated heights of 40 cm (Bridges et al., 2012) and migration rates of ~0.5 m/yr would yield low rates of sand flux (0.1 m^3 m^{-1} yr^{-1}) and abrasion (~0.01–0.70 m/Myr). If persistent, even this modest amount of aeolian abrasion could account for the exhumation of portions of the deltaic deposits since the end of basin aqueous activity in the mid-Hesperian (Rice et al., 2013) and account for local scarp retreat (Williams & Rice, 2017).

If ripple fluxes in SW Melas (Figure 4d) were persistent over time, they would produce similar abrasion rates as Eberswalde (~0.1 m/Myr) and be able to account for some of the 200–500 m of denudation estimated since the approximated end of basin fluvial activity (Quantin et al., 2005; Williams & Weitz, 2014). Similarly, recent crater-based analysis looking at steady exhumation rates of the Melas inner basin estimated comparable rates (0.3–0.9 m/Myr) and concluded erosion out-paced radiolysis of any putative organic matter (Kite & Mayer, 2017).

The downselected Jezero site has active ripples, which may be part of a more significant westward sediment pathway across the crater interior. The Jezero ripples yield fluxes (0.04 m^3 m^{-1} yr^{-1}) and abrasion rates (~0.01–0.30 m/Myr). Prior characterization of the Jezero geology has suggested that the lateral extent and strata thickness of the fluvial deposits was deflated and partially removed (Fassett & Head, 2005; Goudge et al., 2012). Ripple abrasion here could account for exhuming some of the deltaic deposit. Moreover, if the low-flux dunes currently abrading plateau surfaces at moderate rates ~0.1–7.0 m/Myr (Figures 7c and 8e) are representative of past Jezero dunes, exhumation rates would have been greater.

The four remaining sites also exhibit variable signs of erosion and sediment availability. However, the Mawrth Vallis plateau area did not yield clear evidence for local sand transport. The Mawrth candidate site is thus interpreted to have sustained low levels of aeolian erosion other than deflation from wind gusts or dust devils, which must be periodically removing dust and allowing orbital spectral detections. These results would also be relevant to planners of the 2020 ExoMars mission (Bridges, Loizeau, et al., 2017), if young surface exposure ages were a key criteria.

The Nili Fossae site, in contrast, displayed the most unambiguous evidence for local sand transport and erosion with the moderate-flux dunes adjacent to the ellipse. These dunes are estimated to produce high abrasion rates (1.0–47.2 m/Myr) of local trough surfaces. An average of 10 m of erosion per million year period would likely not be a steady state exhumation rate but a snap shot of rates during intermediate obliquity periods. Nevertheless, local aeolian erosion appears to be an important factor for the exposure of geologic units since the Noachian.

The evidence for sand pathways in and around the NE Syrtis ellipse, and the broader area (Figure 8a), suggests that long-term aeolian erosion contributes to local landscape evolution and supports earlier interpretations of erosional windows (e.g., Bramble et al., 2017). The small dunes detected migrating to the north and south of the ellipse yield comparable abrasion rates (0.2–11.1 m/Myr) to what was estimated for Gale crater. These rates, if consistent for ~0.2–10 Myr, would remove the necessary 2 m of overburden for low exposure ages for local rocks.

Finally, the Columbia Hills site produced poor evidence for contemporary sand movement or even regional sand dunes. Although numerous but discrete fields of small ripples occur there, these were interpreted to be dominated by coarse sand and inactive, as was the consensus from analysis by the *Spirit* rover (Sullivan et al., 2008). *Spirit* also encountered smaller impact ripples, which did show measurable displacements. However, this migration was attributed to extreme wind events experienced during the 2007 global dust storm (Sullivan et al., 2008). Nevertheless, if we assume that these small ripples could maintain the 0.4 cm per Sol migration rate over time (~5 m/yr) and are widespread across the Columbia Hills, they would be eroding the surface. With estimated impact heights of 1 cm (1:10th bedform wavelength height is the canonical relationship (Bridges et al., 2012)) these ripples could abrade a maximum of ~0.3 m/Myr. These rates are much higher than earlier in situ and orbital estimates of 2–3 $\times$ 10^{-5} m/Myr for Gusev plains and ~10^{-3} m/Myr for the Columbia Hills (Golombek et al., 2006, 2014), so they may be only representative of high wind events. In conclusion, little compelling evidence was found for even moderate rates of sand erosion at the Columbia Hills site, and long exposure ages for most geologic units would be anticipated.

5.3. Additional Factors Influencing Aeolian Erosion at Mars 2020 Candidate-Landing Sites

Here we discuss interpretations for our generalized results given several factors. Results demonstrate substantial geographic heterogeneity in dune sediment fluxes and extrapolated abrasion rates across the 2020 sites. For context, these reported flux values are often an order of (relative) magnitude less than for dune fields on Earth but similar or larger than earlier reports for Mars (Bridges et al., 2012; Chojnacki et al., 2015, 2017). All of these results deserve some additional consideration, as sand transport and erosion will vary given a number of factors. Perhaps one of the more important variables to consider is climate and how orbital obliquity can significantly influence temperature and pressure, which, in turn, influence winds. Sand abrasion will be greater during periods of higher atmospheric pressure as the threshold friction speed will be reduced along with the greater occurrence of high winds (Armstrong & Leovy, 2005). This was observed from high-frequency seasonal monitoring of the Nili Patera dune field (Ayoub et al., 2014) that showed the greatest ripple fluxes during perihelion (estimated local pressure of 6.3 mbar (Withers, 2012)), while they were lowest during aphelion (5.3 mbar). This modest change in pressure resulted in a threefold increase in sand fluxes (Ayoub et al., 2014). An even greater1.6–2.5-fold increase in atmospheric pressure is expected during the higher orbital obliquity periods that were likely to have occurred in the last several million years (Kieffer & Zent, 1992; Laskar et al., 2004), resulting in higher sand transport rates. For example, doubling the pressure to ~12 mbar would increase fluxes (and abrasion rates) at least an order of magnitude. However, as obliquities increase, so will occurrences of equatorial ground ice (Armstrong & Leovy, 2005; Laskar et al., 2004), which have additional implications for erosion and the potential shielding of geologic units from radiation. Wind regimes can also shift with changes in climate, which are likely to influence sediment pathways and

bedform activity (Chojnacki et al., 2017; Fenton et al., 2015; Golombek et al., 2010). Thus, bedform motion and other associated geomorphic processes on Mars are likely cyclical.

Geologic rock type will also influence erosion rates. This was recognized by earlier studies of Martian sedimentary layered terrains, similar to those at many 2020 sites, which generally lacked small craters implying that some steady erosion is occurring (~1 m/Myr) (Kite & Mayer, 2017; Malin & Edgett, 2000; McEwen et al., 2005). Abrasion rates estimated above will be greater for most sedimentary units at candidate sites, as all estimates above assumed a dense basaltic target material. The lower abrasion susceptibility of softer sedimentary terrains composed of sulfates and softer clays will allow for greater erosion. For example, if laboratory-derived susceptibility values for hydrocal (gypsum cement) (Greeley et al., 1982) were used to reflect a more friable target material, then the abrasion rates generally increase by an order of magnitude. Even some Columbia Hills rock types interpreted as volcanoclastic yield lower rock strengths relative to basaltic materials and will be more susceptible to erosion (Thomson et al., 2013). However, more massive carbonate units displaying relatively high thermal inertia (e.g., Columbia Hills, Jezero, and NE Syrtis) may be more resistant to erosion as compared with poorly consolidated sedimentary units. These are all factors that must be considered for future sampling. It is worth noting the composition of the target rock will also influence the system's overall sedimentary budget. For example, clay minerals (i.e., sheet silicates) will be more susceptible to ejection and suspension, whereas many primary minerals (e.g., pyroxenes and olivine) will be dislodged and likely incorporated into the system.

Other antecedent geomorphic boundary conditions can also affect aeolian processes. For example, dune fluxes in Meridiani Planum appear to be dampened for locations with rugged adjacent topography compared with more modified smoother craters (Chojnacki et al., 2017). This factor may favor more topographically muted sites (e.g., NE Syrtis and Nili Fossae) and allow greater sand transport and erosion. On the other hand, abrasion rates will be an order of magnitude greater for higher sloping rocks encountered within the saltation cloud column (Bridges et al., 2012), so these factors may offset one another. Additionally, if sand coverage is thick enough (~2 m), bedforms (which appear static; e.g., Figures 2d, 5c, and 9c) may also protect the underlying bedrock from radiation and potential radioalysis. This last point may complicate the perceived low erosion rates at some locations (e.g., Holden and Mawrth).

Wind regimes can also be accentuated or muted depending on larger-scale topography. Global analysis of mobile bedforms indicates that many regions adjacent to large topographic dichotomies possess dunes with high sediment fluxes (e.g., Olympia Undae adjacent to the North Polar cap and Hellespontus adjacent to East Hellas) (Banks et al., 2017; Bridges et al., 2011). The Isidis impact basin notably appears to affect large-scale atmospheric flow in the Syrtis Major region with consistent westward sand transport from Nili Patera to Nili Fossae ($>$1,000 km; Figure 1b). In contrast, the high-flux intracrater dunes in extreme NW Arabia Terra near the global dichotomy (Figure 5b) were not found to be representative of dunes in the higher elevation plateau regions of the Mawrth site despite close proximity. Future efforts will be employed in understanding these factors and their overall effect on sand transport across Mars.

Although this study focused on estimating perceived abrasion from mobile, meter-scale (or larger) bedforms from long-baseline image pairs (3–5 Mars years), it is important to acknowledge that other forms of aeolian erosion may be occurring, either underresolved decimeter ripples or direct wind erosion with little entrained sediment involved. Additionally, other erosional and weathering processes contribute to landscape evolution (e.g., thermal stress, aqueous alteration/diagenesis, and mass wasting) but were not considered herein.

6. Conclusions

The Mars 2020 Rover mission is currently seeking a suitable landing site that will address questions regarding past habitability and the potential preservation of biosignatures. The rapid aeolian abrasion of sedimentary deposits, which potentially host ancient habitable environments, may provide the best mechanism for exposing samples containing relatively undegraded organics (Grotzinger et al., 2014). This investigation sought to quantify aeolian activity at the (initial) eight Mars 2020 candidate-landing sites in an effort to better assess erosion and exposure potential at each site.

Results indicate substantial geographic heterogeneity of dune crest fluxes and bedform activity across the eight candidate 2020 landing sites. Evidence for sand availability and contemporary bedform movement suggest that of the three downselected sites, Jezero crater and NE Syrtis showed the most potential for ongoing

erosion and exposure potential of local geology. Potential samples of organic materials at these sites, if present, could have been recently exposed by aeolian abrasion, supplemented by other forms of erosion, as proposed at Gale crater (Farley et al., 2014; Grotzinger et al., 2014). Additional findings from the investigation include the following.

1. Local erosion rates derived from modern dune fluxes at Gale crater were found to be consistent with the sedimentary scarp rates estimated from other techniques by the *Curiosity* team.
2. The Holden and Eberswalde sites showed moderate regional sediment fluxes including for dunes within Holden crater. Although the Holden ellipse area was interpreted to have low contemporary erosion rates, past aeolian erosion likely contributed to terrain inversion.
3. Active ripples at the Eberswalde site, if persistent for protracted periods, could account for local erosion and the evidence for recent scarp retreat from independent analysis.
4. The SW Melas site was found to host migrating sand ripples, which may have contributed to previous estimates of sedimentary deposit and small crater exhumation.
5. Moderate-flux regional dunes near Mawrth Vallis are deemed unrepresentative of the candidate site, which is interpreted to have sustained low levels of aeolian erosion.
6. The Nili Fossae site displayed the most unambiguous evidence for local sand transport and erosion, which would likely yield relatively young exposure ages of potential samples.
7. The Jezero crater and NE Syrtis sites had high regional fluxes and exhibited strong evidence for sediment pathways across their ellipses. Both sites had relatively high estimated contemporary abrasion rates, which would yield low exposure ages if persistent.
8. The Columbia Hills site lacked regional dune fields, and local boundary conditions appear to be only conducive for the formation of currently inactive coarse-grained ripple fields and the limited mobility of smaller impact ripples. Estimated local abrasion rates are relatively low suggesting long exposure ages.

Acknowledgments
Insightful reviews provided by Matthew Golombek and Edwin Kite greatly improved this manuscript and are kindly acknowledged. We would like to thank the students and staff at University of Arizona's HiRISE Operations Center (HiROC) for assistance with imaging targeting and DTM production, particularly Sarah Sutton. We are also grateful for the efforts of the many people responsible for the success of the MRO/HiRISE mission. We would also like to recognize the many science contributions, which were relevant to this study, from the late Nathan Bridges. This research was supported in part by NASA Mars Data Analysis Program grants NNH14ZDA001N (for M. Chojnacki and A. Urso) and NNX14AO96G (for M. Banks). Supporting information is available in the online version of the paper, including supplemental tables, figures, methodology, and animated GIFs. All of the data used for this investigation can be found at the HiRISE website (http://hirise.lpl.arizona.edu/) or the Planetary Data System (http://pds.nasa.gov/).

References

Armstrong, J. C., & Leovy, C. B. (2005). Long term wind erosion on Mars. *Icarus*, *176*(1), 57–74. https://doi.org/10.1016/j.icarus.2005.01.005

Arvidson, R. E., Squyres, S. W., Anderson, R. C., Bell, J. F., Blaney, D., Brückner, J., et al. (2006). Overview of the Spirit Mars Exploration Rover Mission to Gusev Crater: Landing site to Backstay Rock in the Columbia Hills. *Journal of Geophysical Research*, *111*, E02S01. https://doi.org/10.1029/2005JE002499

Ayoub, F., Avouac, J.-P., Newman, C. E., Richardson, M. I., Lucas, A., Leprince, S., & Bridges, N. T. (2014). Threshold for sand mobility on Mars calibrated from seasonal variations of sand flux. *Nature Communications*, 5. https://doi.org/10.1038/ncomms6096

Banks, M. E., Fenton, L. K., Bridges, N. T., Geissler, P. E., Chojnacki, M., Silvestro, S., & Zimbelman, J. R. (2017). Patterns in mobility and modification of middle and high latitude Southern Hemisphere dunes (p. Abstract #2918). Presented at the 48th Lunar and Planetary Science Conference, Houston: Lunar and Planetary Institute. Retrieved from http://www.lpi.usra.edu/meetings/lpsc2017/pdf/2918.pdf

Banks, M. E., Geissler, P. E., Bridges, N. T., Russell, P., Silvestro, S., Chojnacki, M., et al. (2015). Emerging global trends in eolian bedform mobility on Mars (p. Abstract #8036). Presented at the Fourth International Planetary Dunes Workshop:Integrating Models, Remote Sensing, and Field Data, Houston: Lunar and Planetary Institute. Retrieved from http://www.lpi.usra.edu/meetings/dunes2015/pdf/8036.pdf

Baratoux, D., Pinet, P., Gendrin, A., Kanner, L., Mustard, J., Daydou, Y., et al. (2007). Mineralogical structure of the subsurface of Syrtis Major from OMEGA observations of lobate ejecta blankets. *Journal of Geophysical Research*, *112*, E08S05. https://doi.org/10.1029/2007JE002890

Bibring, J. P., Langevin, Y., Gendrin, A., Gondet, B., Poulet, F., Berthe, M., et al. (2005). Mars surface diversity as revealed by the OMEGA/Mars Express observations. *Science*, *307*(5715), 1576–1581. https://doi.org/10.1126/Science.1108806

Bishop, J. L., Dobrea, E. Z. N., McKeown, N. K., Parente, M., Ehlmann, B. L., Michalski, J. R., et al. (2008). Phyllosilicate diversity and past aqueous activity revealed at Mawrth Vallis, Mars. *Science*, *321*(5890), 830–833. https://doi.org/10.1126/Science.1159699

Bourke, M., Edgett, K., & Cantor, B. (2008). Recent eolian dune change on Mars. *Geomorphology*, *94*(1–2), 247–255. https://doi.org/10.1016/j.geomorph.2007.05.012

Bramble, M. S., Mustard, J. F., & Salvatore, M. R. (2017). The geological history of Northeast Syrtis Major, Mars. *Icarus*, *293*, 66–93. https://doi.org/10.1016/j.icarus.2017.03.030

Bridges, J., Loizeau, D., Sefton-Nash, E., Vago, J., Williams, R. M. E., Balme, M., et al. (2017). Selection and characterization of the ExoMars 2020 Rover landing sites. In *48th Lunar and Planetary Science Conference* (p. Abstract #2378). Houston: Lunar and Planetary Institute. Retrieved from http://www.lpi.usra.edu/meetings/lpsc2017/pdf/2378.pdf

Bridges, N. T., Ayoub, F., Avouac, J.-P., Leprince, S., Lucas, A., & Mattson, S. (2012). Earth-like sand fluxes on Mars. *Nature*, *485*(7398), 339–342. https://doi.org/10.1038/nature11022

Bridges, N. T., Bourke, M. C., Geissler, P. E., Banks, M. E., Colon, C., Diniega, S., et al. (2011). Planet-wide sand motion on Mars. *Geology*, *40*(1), 31–34. https://doi.org/10.1130/G32373.1

Bridges, N. T., Geissler, P., Silvestro, S., & Banks, M. (2013). Bedform migration on Mars: Current results and future plans. *AeolianResearch*, *9*, 133–151. https://doi.org/10.1016/j.aeolia.2013.02.004

Bridges, N. T., Sullivan, R., Newman, C. E., Navarro, S., Van Beek, J., Ewing, R. C., et al. (2017). Martian eolian activity at the Bagnold Dunes, Gale crater: The view from the surface and orbit. *Journal of Geophysical Research: Planets*, *122*, 2077–2110. https://doi.org/10.1002/2017JE005263

Chojnacki, M., Burr, D. M., & Moersch, J. E. (2014). Valles Marineris dune fields as compared with other Martian populations: Diversity of dune compositions, morphologies, and thermophysical properties. *Third Planetary Dunes Systems*, *230*, 96–142. https://doi.org/10.1016/j.icarus.2013.08.018

Chojnacki, M., Burr, D. M., Moersch, J. E., & Michaels, T. I. (2011). Orbital observations of contemporary dune activity in Endeavor crater, Meridiani Planum, Mars. *Journal of Geophysical Research*, *116*, E00F19. https://doi.org/10.1029/2010JE003675

Chojnacki, M., Johnson, J. R., Moersch, J. E., Fenton, L. K., Michaels, T. I., & Bell, J. F. III (2015). Persistent eolian activity at Endeavour crater, Meridiani Planum, Mars: New observations from orbit and the surface. *Dynamic Mars*, *251*, 275–290. https://doi.org/10.1016/j.icarus.2014.04.044

Chojnacki, M., Urso, A. C., Fenton, L. K., & Michaels, T. I. (2017). Eolian dune sediment flux heterogeneity in Meridiani Planum, Mars. *Aeolian Research*, *26*, 73–88. https://doi.org/10.1016/j.aeolia.2016.07.004

Christensen, P., Engle, E., Anwar, S., Dickenshield, S., Noss, D., & Weiss-Malik, M. (2009). *JMARS—A planetary GIS*. Abstract IN22A-06 Presented at the 2009 AGU Fall Meeting, San Francisco, CA.

Crumpler, L. S., Arvidson, R. E., Squyres, S. W., McCoy, T., Yingst, A., Ruff, S., et al. (2011). Field reconnaissance geologic mapping of the Columbia Hills, Mars, based on Mars Exploration Rover Spirit and MRO HiRISE observations. *Journal of Geophysical Research*, *116*, E00F24. https://doi.org/10.1029/2010JE003749

Day, M., & Kocurek, G. (2015). Observations of an eolian landscape: From surface to orbit in Gale Crater. *Icarus*. https://doi.org/10.1016/j.icarus.2015.09.042

Edwards, C. S., & Ehlmann, B. L. (2015). Carbon sequestration on Mars. *Geology*, *43*(10), 863–866. https://doi.org/10.1130/G36983.1

Ehlmann, B. L., Mustard, J. F., Fassett, C. I., Schon, S. C., Head, J. W., Marais, D. J. D., et al. (2008). Clay minerals in delta deposits and organic preservation potential on Mars. *Nature Geoscience*, *1*(6), 355–358. https://doi.org/10.1038/Ngeo207

Ehlmann, B. L., Mustard, J. F., Swayze, G. A., Clark, R. N., Bishop, J. L., Poulet, F., et al. (2009). Identification of hydrated silicate minerals on Mars using MRO-CRISM: Geologic context near Nili Fossae and implications for aqueous alteration. *Journal of Geophysical Research*, *114*, E00D08. https://doi.org/10.1029/2009JE003339

Farley, K. A., Malespin, C., Mahaffy, P., Grotzinger, J. P., Vasconcelos, P. M., Milliken, R. E., et al. (2014). In situ radiometric and exposure age dating of the Martian surface. *Science*, *343*(6169). 1247166–1247166. https://doi.org/10.1126/science.1247166

Fassett, C. I., & Head, J. W. (2005). Fluvial sedimentary deposits on Mars: Ancient deltas in a crater lake in the Nili Fossae region: FLUVIAL SEDIMENTARY DEPOSITS ON MARS. *Geophysical Research Letters*, *32*, L14201. https://doi.org/10.1029/2005GL023456

Fenton, L. K., Michaels, T. I., & Chojnacki, M. (2015). Late Amazonian eolian features, gradation, wind regimes, and sediment state in the vicinity of the Mars exploration rover Opportunity, Meridiani Planum, Mars. *Aeolian Research*, *16*, 75–99. https://doi.org/10.1016/j.aeolia.2014.11.004

Geissler, P. E., & Wilgus, J. T. (2016). The morphology of transverse aeolian ridges on Mars. *Aeolian Research*. https://doi.org/10.1016/j.aeolia.2016.08.008

Golombek, M. P., Grant, J., Kipp, D., Vasavada, A., Kirk, R., Fergason, R., et al. (2012). Selection of the Mars Science Laboratory Landing Site. *Space Science Reviews*, *170*(1–4), 641–737. https://doi.org/10.1007/s11214-012-9916-y

Golombek, M. P., Grant, J. A., Crumpler, L. S., Greeley, R., Arvidson, R. E., Bell, J. F., et al. (2006). Erosion rates at the Mars Exploration Rover landing sites and long-term climate change on Mars. *Journal of Geophysical Research*, *111*, E12S10. https://doi.org/10.1029/2006JE002754

Golombek, M. P., Otero, R. E., Heverly, M. C., Ono, M., Williford, K. H., Rothrock, B., et al. (2017). Characterization of Mars Rover 2020 prospective landing sites leading up to the second downselection. In 48th *Lunar and Planetary Science Conference* (p. Abstract #2333). Houston: Lunar and Planetary Institute. Retrieved from http://www.lpi.usra.edu/meetings/lpsc2017/pdf/2333.pdf

Golombek, M. P., Robinson, K., McEwen, A., Bridges, N., Ivanov, B., Tornabene, L., & Sullivan, R. (2010). Constraints on ripple migration at Meridiani Planum from Opportunity and HiRISE observations of fresh craters. *Journal of Geophysical Research*, *115*, E00F08. https://doi.org/10.1029/2010JE003628

Golombek, M. P., Warner, N. H., Ganti, V., Lamb, M. P., Parker, T. J., Fergason, R. L., & Sullivan, R. (2014). Small crater modification on Meridiani Planum and implications for erosion rates and climate change on Mars: Small Crater Modification on Mars. *Journal of Geophysical Research: Planets*, *119*, 2522–2547. https://doi.org/10.1002/2014JE004658

Goudge, T. A., Head, J. W., Mustard, J. F., & Fassett, C. I. (2012). An analysis of open-basin lake deposits on Mars: Evidence for the nature of associated lacustrine deposits and post-lacustrine modification processes. *Icarus*, *219*(1), 211–229. https://doi.org/10.1016/j.icarus.2012.02.027

Grant, J. A., Irwin, R. P., Grotzinger, J. P., Milliken, R. E., Tornabene, L. L., McEwen, A. S., et al. (2008). HiRISE imaging of impact megabreccia and sub-meter aqueous strata in Holden Crater, Mars. *Geology*, *36*(3), 195. https://doi.org/10.1130/G24340A.1

Grant, J. A., & Wilson, S. A. (2011). Late alluvial fan formation in southern Margaritifer Terra, Mars. *Geophysical Research Letters*, *38*, L08201. https://doi.org/10.1029/2011GL046844

Greeley, R., Arvidson, R. E., Barlett, P. W., Blaney, D., Cabrol, N. A., Christensen, P. R., et al. (2006). Gusev crater: Wind-related features and processes observed by the Mars Exploration Rover Spirit. *Journal of Geophysical Research*, *111*, E02S09. https://doi.org/10.1029/2005JE002491

Greeley, R., Leach, R. N., Williams, S. H., White, B. R., Pollack, J. B., Krinsley, D. H., & Marshall, J. R. (1982). Rate of wind abrasion on Mars. *Journal of Geophysical Research*, *87*(B12), 10,009–10,024. https://doi.org/10.1029/JB087iB12p10009

Grotzinger, J. P., & Milliken, R. E. (2012). *Sedimentary geology of Mars*. Tulsa, OK: SEPM (Society for Sedimentary Geology). Retrieved from http://sp.sepmonline.org/content/sepspecpub/sepsp102/1.toccontent/102

Grotzinger, J. P., Sumner, D. Y., Kah, L. C., Stack, K., Gupta, S., Edgar, L., et al. (2014). A habitable fluvio-lacustrine environment at Yellowknife Bay, Gale Crater, Mars. *Science*, *343*(6169). https://doi.org/10.1126/science.1242777

Hayward, R. K., Fenton, L. K., & Titus, T. N. (2014). Mars Global Digital Dune Database (MGD3): Global dune distribution and wind pattern observations. *Icarus*, *230*, 38–46. https://doi.org/10.1016/j.icarus.2013.04.011

Hoefen, T. M., Clark, R. N., Bandfield, J. L., Smith, M. D., Pearl, J. C., & Christensen, P. R. (2003). Discovery of olivine in the Nili Fossae region of Mars. *Science*, *302*(5645), 627–630.

Kieffer, H. H., & Zent, A. P. (1992). Quasi-periodic climatic change on Mars. In H. H. Kieffer, et al. (Eds.), *Mars* (pp. 1180–1220). Tucson: University of Arizona Press.

Kite, E. S., & Mayer, D. P. (2017). Mars sedimentary rock erosion rates constrained using crater counts, with applications to organic-matter preservation and to the global dust cycle. *Icarus*, *286*, 212–222. https://doi.org/10.1016/j.icarus.2016.10.010

Lancaster, N. (1988). Controls of eolian dune size and spacing. *Geology*, *16*(11), 972. https://doi.org/10.1130/0091-7613(1988)016%3C0972:COEDSA%3E2.3.CO;2

Lapotre, M. G. A., Ewing, R. C., Lamb, M. P., Fischer, W. W., Grotzinger, J. P., Rubin, D. M., et al. (2016). Large wind ripples on Mars: A record of atmospheric evolution. *Science*, *353*(6294), 55–58. https://doi.org/10.1126/science.aaf3206

Laskar, J., Correia, A. C. M., Gastineau, M., Joutel, F., Levrard, B., & Robutel, P. (2004). Long term evolution and chaotic diffusion of the insolation quantities of Mars. *Icarus*, *170*(2), 343–364. https://doi.org/10.1016/j.icarus.2004.04.005

Lewis, K. W., & Aharonson, O. (2006). Stratigraphic analysis of the distributary fan in Eberswalde crater using stereo imagery. *Journal of Geophysical Research: Planets*, *111*, E06001. https://doi.org/10.1029/2005JE002558

Loizeau, D., Mangold, N., Poulet, F., Bibring, J. P., Gendrin, A., Ansan, V., et al. (2007). Phyllosilicates in the Mawrth Vallis region of Mars. *Journal of Geophysical Research*, *112*, E08s08. https://doi.org/10.1029/2006JE002877

Malin, M. C., Bell, J. F., Cantor, B. A., Caplinger, M. A., Calvin, W. M., Clancy, R. T., et al. (2007). Context Camera investigation on board the Mars Reconnaissance Orbiter. *Journal of Geophysical Research*, *112*, E05S04. https://doi.org/10.1029/2006JE002808

Malin, M. C., & Edgett, K. S. (2000). Sedimentary rocks of early Mars. *Science*, *290*(5498), 1927–1937.

Mangold, N., Quantin, C., Ansan, V., Delacourt, C., & Allemand, P. (2004). Evidence for precipitation on Mars from Dendritic Valleys in the Valles Marineris Area. *Science*, *305*(5680), 78–81. https://doi.org/10.1126/science.1097549

McEwen, A. S., Chojnacki, M., Miyamoto, H., Hemmi, R., Weitz, C., Williams, R., et al. (2015). Landing site and exploration zone in Eastern Melas Chasma. In *First Landing Site/Exploration Zone Workshop for Human Missions to the Surface of Mars* (p. Abstract #1007). Houston: Lunar and Planetary Institute. Retrieved from http://www.lpi.usra.edu/meetings/explorationzone2015/pdf/1007.pdf

McEwen, A. S., Eliason, E. M., Bergstrom, J. W., Bridges, N. T., Hansen, C. J., Delamere, W. A., et al. (2007). Mars Reconnaissance Orbiter's High Resolution Imaging Science Experiment (HiRISE). *Journal of Geophysical Research*, *112*, E05S02. https://doi.org/10.1029/2005JE002605

McEwen, A. S., Preblich, B. S., Turtle, E. P., Artemieva, N. A., Golombek, M. P., Hurst, M., et al. (2005). The rayed crater Zunil and interpretations of small impact craters on Mars. *Icarus*, *176*(2), 351–381.

Metz, J. M., Grotzinger, J. P., Mohrig, D., Milliken, R., Prather, B., Pirmez, C., et al. (2009). Sublacustrine depositional fans in southwest Melas Chasma: SUBLACUSTRINE DEPOSITIONAL FANS. *Journal of Geophysical Research*, *114*, E10002. https://doi.org/10.1029/2009JE003365

Michalski, J. R., & Noe Dobrea, E. Z. (2007). Evidence for a sedimentary origin of clay minerals in the Mawrth Vallis region, Mars. *Geology*, *35*(10), 951–954. https://doi.org/10.1130/G23854a.1

Milliken, R. E., & Bish, D. L. (2010). Sources and sinks of clay minerals on Mars. *Philosophical Magazine*, *90*(17–18), 2293–2308. https://doi.org/10.1080/14786430903575132

Moore, J. M., & Howard, A. D. (2005). Large alluvial fans on Mars. *Journal of Geophysical Research*, *110*, E04005. https://doi.org/10.1029/2004JE002352

Morris, R. V., Ruff, S. W., Gellert, R., Ming, D. W., Arvidson, R. E., Clark, B. C., et al. (2010). Identification of carbonate-rich outcrops on Mars by the Spirit Rover. *Science*, *329*(5990), 421–424. https://doi.org/10.1126/science.1189667

Mustard, J. F., Murchie, S. L., Pelkey, S. M., Ehlmann, B. L., Milliken, R. E., Grant, J. A., et al. (2008). Hydrated silicate minerals on mars observed by the Mars reconnaissance orbiter CRISM instrument. *Nature*, *454*(7202), 305–309. https://doi.org/10.1038/Nature07097

Mustard, J. F., Poulet, F., Head, J. W., Mangold, N., Bibring, J. P., Pelkey, S. M., et al. (2007). Mineralogy of the Nili Fossae region with OMEGA/Mars Express data: 1. Ancient impact melt in the Isidis Basin and implications for the transition from the Noachian to Hesperian. *Journal of Geophysical Research*, *112*, E08S03. https://doi.org/10.1029/2006JE002834

Mustard, J. F., Adler, M., Allwood, A., Bass, D. S., Beaty, D. W., Bell, J. F. III, et al. (2013). Report of the Mars 2020 Science Definition Team (154 pp.). posted July, 2013, by the Mars Exploration Program Analysis Group (MEPAG) at http://mepag.jpl.nasa.gov/reports/MEP/Mars_2020_SDT_Report_Final.pdf

Poulet, F., Bibring, J. P., Mustard, J. F., Gendrin, A., Mangold, N., Langevin, Y., et al. (2005). Phyllosilicates on Mars and implications for early martian climate. *Nature*, *438*(7068), 623–627. https://doi.org/10.1038/Nature04274

Quantin, C., Allemand, P., Mangold, N., Dromart, G., & Delacourt, C. (2005). Fluvial and lacustrine activity on layered deposits in Melas Chasma, Valles Marineris, Mars. *Journal of Geophysical Research*, *110*, E12S19. https://doi.org/10.1029/2005JE002440

Rice, M. S., Bell, J. F., Gupta, S., Warner, N. H., Goddard, K., & Anderson, R. S. (2013). A detailed geologic characterization of Eberswalde crater, Mars. *Mars*, *8*, 15–57. https://doi.org/10.1555/mars.2013.0002

Rice, M. S., Gupta, S., Bell, J. F., & Warner, N. H. (2011). Influence of fault-controlled topography on fluvio-deltaic sedimentary systems in Eberswalde crater, Mars. *Geophysical Research Letters*, *38*, L16203. https://doi.org/10.1029/2011GL048149

Ruff, S. W., & Farmer, J. D. (2016). Silica deposits on Mars with features resembling hot spring biosignatures at El Tatio in Chile. *Nature Communications*, *7*, 13554. https://doi.org/10.1038/ncomms13554

Ruff, S. W., Farmer, J. D., Calvin, W. M., Herkenhoff, K. E., Johnson, J. R., Morris, R. V., et al. (2011). Characteristics, distribution, origin, and significance of opaline silica observed by the Spirit rover in Gusev crater, Mars. *Journal of Geophysical Research*, *116*, E00F23. https://doi.org/10.1029/2010JE003767

Ruff, S. W., Farmer, J. D., Rice, J. W., & Longo, A. (2017). Seeking signs of past microbial life in the Columbia Hills. In *Mars* 20203rd Landing Site Workshop. Pasadena, CA. Retrieved fromhttps://marsnext.jpl.nasa.gov/workshops/wkshp_2017_02.cfm

Silvestro, S., Fenton, L. K., Vaz, D. A., Bridges, N. T., & Ori, G. G. (2010). Ripple migration and dune activity on Mars: Evidence for dynamic wind processes. *Geophysical Research Letters*, *37*, L20203. https://doi.org/10.1029/2010GL044743

Silvestro, S., Vaz, D. A., Ewing, R. C., Rossi, A. P., Fenton, L. K., Michaels, T. I., et al. (2013). Pervasive aeolian activity along rover Curiosity's traverse in Gale Crater, Mars. *Geology*, *41*(4), 483–486. https://doi.org/10.1130/G34162.1

Squyres, S. W., Arvidson, R. E., Baumgartner, E. T., Bell, J. F., Christensen, P. R., Gorevan, S., et al. (2003). Athena Mars rover science investigation. *Journal of Geophysical Research*, *108*(E12). 8062. https://doi.org/10.1029/2003JE002121

Sullivan, R., Arvidson, R., Bell, J. F., Gellert, R., Golombek, M., Greeley, R., et al. (2008). Wind-driven particle mobility on Mars: Insights from Mars Exploration Rover observations at "El Dorado" and surroundings at Gusev Crater. *Journal of Geophysical Research*, *113*, E06S07. https://doi.org/10.1029/2008JE003101

Thomson, B. J., Bridges, N. T., Cohen, J., Hurowitz, J. A., Lennon, A., Paulsen, G., & Zacny, K. (2013). Estimating rock compressive strength from Rock Abrasion Tool (RAT) grinds. *Journal of Geophysical Research: Planets*, *118*, 1233–1244. https://doi.org/10.1002/jgre.20061

Weitz, C. M. (2003). Geology of the Melas Chasma landing site for the Mars Exploration Rover mission. *Journal of Geophysical Research*, *108*(E12), 2082. https://doi.org/10.1029/2002JE002022

Williams, R. M. E., & Rice, M. S. (2017). Evaluating the proposed Mars 2020 sedimentary landing sites for ongoing exhumation and recent exposure. In *Mars 2020 3rd Landing Site Workshop*. Pasadena, CA. Retrieved from https://marsnext.jpl.nasa.gov/workshops/wkshp_2017_02.cfm

Williams, R. M. E., & Weitz, C. M. (2014). Reconstructing the aqueous history within the southwestern Melas basin, Mars: Clues from stratigraphic and morphometric analyses of fans. *Icarus*, *242*, 19–37. https://doi.org/10.1016/j.icarus.2014.06.030

Withers, P. (2012). Empirical estimates of Martian surface pressure in support of the landing of Mars Science Laboratory. *Space Science Reviews*, *170*(1–4), 837–860. https://doi.org/10.1007/s11214-012-9876-2

Wray, J. J., Ehlmann, B. L., Squyres, S. W., Mustard, J. F., & Kirk, R. L. (2008). Compositional stratigraphy of clay-bearing layered deposits at Mawrth Vallis, Mars. *Geophysical Research Letters*, *35*, L12202. https://doi.org/10.1029/2008GL034385